NASA CR-185212

PLASMA CONTACTOR RESEARCH - 1989

Prepared for

LEWIS RESEARCH CENTER

NATIONAL AERONAUTICS AND SPACE ADMINISTRATION

Grant NAG 3-776

Annual Report

John D. Williams

February 1990

Approved by

Paul J. Wilbur
Department of Mechanical Engineering
Colorado State University
Fort Collins, Colorado 80523

NASA
National Aeronautics and Space Administration

Report Documentation Page

1. Report No.	2. Government Accession No.	3. Recipient's Catalog No.
NASA CR-185212		

4. Title and Subtitle

Plasma Contactor Research - 1989

5. Report Date
Jan. 1990

6. Performing Organization Code

7. Author(s)
John D. Williams
Paul J. Wilbur

8. Performing Organization Report No.

10. Work Unit No.

9. Performing Organization Name and Address
Department of Mechanical Engineering
Colorado State University
Fort Collins, CO 80523

11. Contract or Grant No.

13. Type of Report and Period Covered
Annual
Jan. 1, 1989 - Jan. 1,1990

12. Sponsoring Agency Name and Address
National Aeronautics and Space Administration
Washington, D.C. 20546

14. Sponsoring Agency Code

15. Supplementary Notes

Grant Monitors- Joel T. Galofaro
Dale Ferguson
NASA Lewis Research Center
Cleveland, OH 44135

16. Abstract

The characteristics of double layers observed by researchers investigating magnetospheric phenomena are contrasted to those observed in plasma contacting experiments. Experiments in the electron collection mode of the plasma contacting process were performed and the results confirm a simple model of this process for current levels ranging to 3 A. Experimental results were also obtained in a study of the process of electron emission from a hollow cathode plasma contactor. High energy ions are observed coming from the cathode in addition to the electrons and a phenomenological model that suggests a mechanism by which this could occur is presented. Experimental results showing the effects of the design parameters of the ambient plasma simulator on the plasma potential, electron temperature, electron density and plasma noise levels induced in plasma contacting experiments are presented. A preferred simulator design is selected on the basis of these results.

17. Key Words (Suggested by Author(s))	18. Distribution Statement
Hollow Cathode Plasma Contactor	Unclassified-Unlimited

19. Security Classif. (of this report)	20. Security Classif. (of this page)	21. No of pages	22. Price*
Unclassified	Unclassified	71	

NASA FORM 1626 OCT 86

*For sale by the National Technical Information Service, Springfield, Virginia 22161

TABLE OF CONTENTS

LIST OF FIGURES

PLASMA CONTACTOR RESEARCH

John D. Williams

INTRODUCTION

A plasma contactor is a device that exchanges current with an ambient plasma. Ground-based experiments suggest that a double layer will form between the ambient plasma and the high density plasma close to a contactor collecting electrons and a large fraction of the potential difference between the contactor and the ambient plasma will develop across this double layer [1,2]. A double layer is essentially two adjacent layers of charge; one, a positive layer at the edge of the high potential plasma (the high density plasma, in the example just mentioned) and the other negative layer at the edge of the low potential plasma (the ambient plasma). The substantial voltage drops, which can develop across this double layer region, are generally undesirable because they represent a power loss. Examples of particularly critical applications of plasma contactors, in which large double layer voltage drops could be disastrous include those involving electrodynamic tethers [3] and on spacecraft from which high current, high energy charged particle beams are being ejected [4].

Typical Results of Plasma Contactor Experiments

The potential variation observed between a plasma contactor collecting electrons and a second contactor supplying electrons to an ambient plasma (the emitter) is shown qualitatively in Fig. 1. The

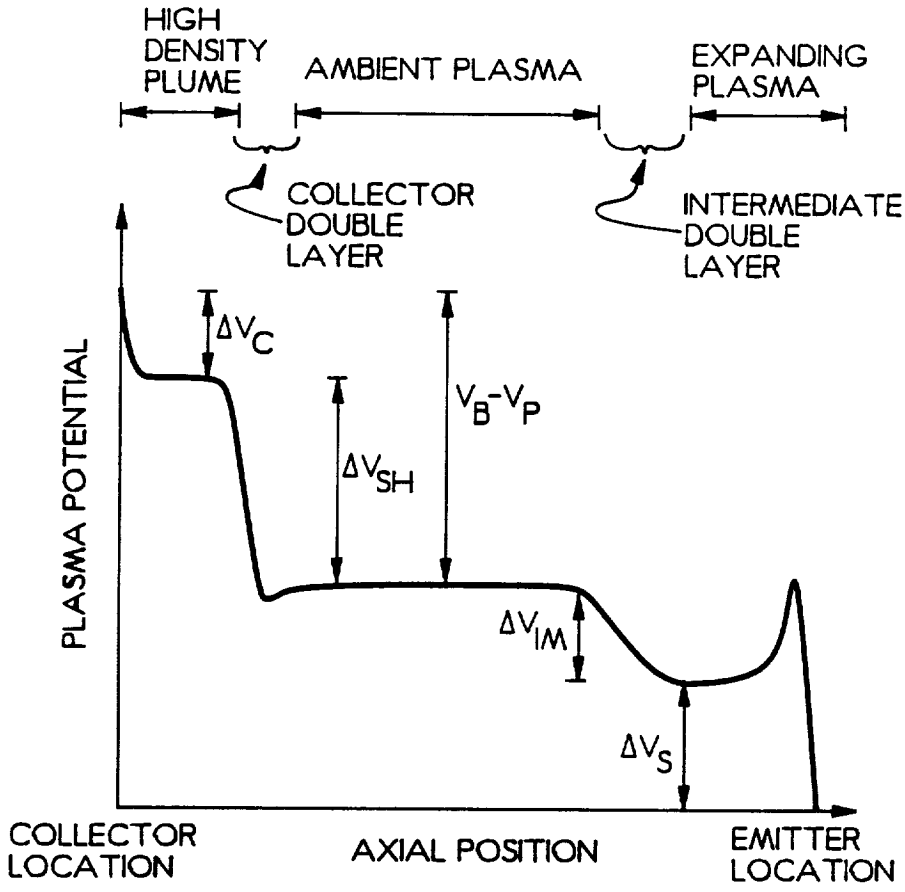

ΔV_C - POTENTIAL DIFFERENCE BETWEEN THE COLLECTOR ANODE AND THE SURROUNDING PLASMA (THE HIGH DENSITY PLUME)

ΔV_{SH} - POTENTIAL DIFFERENCE BETWEEN THE HIGH DENSITY PLUME AND THE AMBIENT PLASMA

ΔV_{IM} - POTENTIAL DIFFERENCE ACROSS INTERMEDIATE DOUBLE LAYER

ΔV_S - POTENTIAL DIFFERENCE BETWEEN THE EMITTER CATHODE AND THE EXPANDING PLASMA REGION

Fig. 1 Plasma Potential Profile Nomenclature

collector is biased positive of the ambient plasma and is collecting an electron current while the emitter is biased negative of the ambient plasma and is emitting an equal electron current. The various potential drops are defined at the bottom of the figure, and the names that have been given to the important regions are defined at the top of the figure. Typically, the high density plume potential is close to the collector anode potential (i.e. $\Delta V_C \sim 0$) and, consequently, the voltage drop experienced across the collector double layer constitutes a large fraction of the potential difference between the collector and the ambient plasma (V_B-V_P: V_B is the potential difference applied between the emitter cathode and the collector anode, and V_P is the potential of the ambient plasma measured relative to the emitter cathode).

A second double layer (the intermediate double layer) is shown between the expanding plasma (flowing from the emitter) and the ambient plasma. The potential drop across it, which is typically 10 to 15 V in our experiments, was originally considered to be due to a vacuum tank wall interaction. However, Vannaroni, et.al. [5] have reported the same structure in separate plasma contactor experiments carried out in another facility. They have argued that this double layer is associated with the electron collection process itself and that multiple double layers may be observed in space applications of plasma contactors as well. It is noted in this regard that multiple double layers have been observed in a number of experiments [6,7].

The potential hill shown near the emitter is probably due to a large ionization rate occurring in this region. Possible explanations of this phenomena are included elsewhere in this report.

Review of Double Layer Experiments and Comparison with Plasma Contactor Experiments

A very thorough review of experimental work on double layers is given by Hershkowitz [6]. For the most part, double layer experiments have been conducted in triple plasma devices, but many double layer experiments have also been conducted in discharge tubes and Q-machines (see also [6] and references therein). Triple plasma devices consist of two plasma sources (equipped with fine wire plasma extraction grids) and a target region. The two plasma sources face each other and are separated by the target region. By biasing the two sources with respect to one another and controlling the amount of plasma that is released by each, it is possible to form a double layer (sometimes more than one) in the target region. In general, the results of these tests and theoretical studies have shown that a minimum of four species of particles are involved in stable double layers. These four species include ions and electrons that are accelerated through the double layer from the high and low potential plasmas, respectively ("free" particles); and ions and electrons that are reflected from the double layer and (generally) remain in the low and high potential plasmas, respectively ("trapped" particles).

The study of double layers and their formation has generally been motivated by the postulate that double layer structures formed in the magnetosphere generate high energy electron beams which are responsible for auroral displays. In order to study this proposal, many researchers turned to the triple plasma device for reasons that reflect its 1) relatively simple operation, 2) provisions for some control over the distribution of trapped and free particles, and 3) low target plasma

densities which ensure rather large double layer regions (several cm in extent). Most of these researchers have been interested in classifying the high and low potential plasmas and then working out models that describe the double layer phenomena in terms of parameters that describe these plasmas [6,7,8,9,10,11]. Unfortunately, few double layer researchers are interested in the magnitudes of the currents or current densities that flow between the high and low potential plasmas at potential differences typical of plasma contacting applications. In fact the currents that flow or the effective impedance between the two plasmas is typically not given, and in one double layer experiment potential structures have been observed when no net current is flowing through the double layer region [12]. Consequently, much of this work cannot be applied directly to quantify the performance of a plasma contactor.

However, the phenomena inherent in plasma contactor experiments in which double layers are observed has also been observed by these double layer experimenters. For example, plasma property data taken in the high density plume (see Fig. 1) has indicated the presence of a high energy electron beam. This beam forms because ambient plasma electrons are accelerated through the collector double layer into the high density plume region. In addition, high energy ions are detected in the ambient plasma. These ions are presumably accelerated through the double layer into the ambient plasma from the high density plume region. The contactor double layer has been shown to be two (or maybe three) dimensional (a feature which was also observed in double layer experiments by Baker, et.al., [8]), but can frequently be described adequately in spherical coordinates [1, 14]. A simple model of

spherical double layers was presented by Wei and Wilbur [15] and it seems to relate the collector double-layer current, voltage and geometrical factors reasonably well. Another simple extension of this model and some experimental verification has also been accomplished [16]. This model assumes that the ions and electrons counterstreaming through the double layer are flowing at their space charge-limited values. The performance of the plasma contactor has been shown to improve (exhibit lower impedance) when electrons accelerated through the double layer from the ambient plasma can ionize neutral atoms in the high density plume [17]. This performance improvement has been related to higher ion production rates which facilitate greater ion current flow from the high density plume through the double layer. In addition to these simple models of the plasma contacting process, more detailed numerical studies have been performed which correlate well with experimental results [14] and confirm the essential features of the model. This work is particularly important because it enables one to not only determine the voltage drop between two laboratory plasmas, but also to calculate the voltage drop that will develop between a plasma contactor plume and a space plasma.

The collector double layer potential drop and position have been observed to be affected by contactor flowrate, anode size, and electron collection current and double layer potential drops measured under typical experimental conditions have been in the range from 10 to 80V [1]. Although changes in these parameters did not affect the intermediate double layer as much, they did cause it to reposition itself and thereby adjust the spatial extent of the ambient and expanding plasma regions. Typically, the electron temperature in the

high density plume was about 4 eV, and when this temperature is used to normalize ΔV_C (i.e. $\Delta\phi = e\Delta V_C/kT_e$) values of double layer strength ($\Delta\phi$) ranging from 2 to 20 have been observed. This strength range has been classified by Hershkowitz as weak (<10) to strong (>10) [6]. In addition to the properties listed above, plasma densities on the high potential side of the double layer have been observed to be higher than those on the low potential side (for both the intermediate and collector double layers). This property of plasma density enhancement across double layers has been observed by many other researchers [6,7,8,9,11] and it has been related in part to the shape of the double layer [8].

In addition to density differences, electron temperature differences have been observed across double layers. For example, the high density plume typically contains both Maxwellian electrons at a temperature between 2 and 4 eV and a group of streaming high energy electrons, while the ambient plasma contains mostly Maxwellian electrons which exhibit a temperature between 5 and 7 eV. In this case the temperature of the electrons in the higher potential plasma (the high density plume) is less than that in the lower potential one. This result has also been observed by Guyot and Hollenstein [7]. Across the intermediate double layer, on the other hand, one observes the more typical situation, a higher electron temperature in the higher potential (ambient) plasma than in the lower potential (expanding) plasma. Chan, et.al. [18] discuss this apparent inconsistency in more detail, and suggest that while some types of double layers might shield two plasmas thermally, other plasma conditions might enhance thermal conduction across them.

Due to the presence of electron and ion beams in the high and low potential plasmas, various plasma instabilities can develop, grow, and cause large amplitude, turbulent electrostatic fluctuations. Some double layer researchers have looked at these fluctuations and found that, typically, low frequency ion-acoustic (ion beam or possibly drifting electron-induced) instabilities are important in the low potential plasma, while high frequency electron-beam instabilities affect the high potential plasma [6,7]. Sometimes the turbulence is important in determining the characteristics of the double layer and other times it does not affect the double layer [6,11]. Regardless of its importance in double layer phenomena, turbulence does exist in both the high and low potential plasmas and it can affect the accuracy and reliability of plasma diagnostics. It has generally been found that emissive probes [6,19] give the best plasma potential measurements. Typically the plasma potential is found first using the emissive probe, and then Langmuir probes are used to characterize the electron energy distribution. In addition to emissive and Langmuir probes, retarding potential analyzers [8,20] can be used to measure the characteristics of the ions and electrons in the various plasmas. All of these probes can be affected by the noise (turbulence) levels present in a plasma, but Langmuir probes are especially vulnerable to errors [21, 22]. Some noise data have been recorded in the experiments being reported here and while the levels are high, they are comparable to those reported in other double layer experiments [7]. The noise level can be reduced by selecting a suitable (quiet and stable) device to generate the ambient plasma. Attempts to do this will be discussed in more detail later in this report.

General Discussion of Report

Experiments have been conducted in which the energy distribution of ions emitted from a region surrounding plasma contactors operating in the electron emission and electron collection modes were measured. As discussed previously, a contactor and its associated plasma plume biased positive with respect to an ambient plasma will collect electrons from and emit ions to that ambient plasma [1]. An investigation of high electron collection current (up to ~3 A) has been performed and is included as part of this report. The motivation for these tests was provided by another plasma contactor study [2] which suggested that the simple electron collection model of Williams and Wilbur [16] was invalid at high electron collection currents (>1 A).

Additional experiments described in this report show that relatively high energy ions were also found to be streaming from a contactor emitting electrons. These ions were identified using a retarding potential analyzer (RPA) and initially it seemed unlikely that high energy ions would be emitted from a contactor which was also emitting electrons. A mechanism was subsequently postulated, which involves a high rate of ionization by electrons being drawn from the hollow cathode orifice that creates a region of high positive space charge and as a consequence a high positive potential immediately downstream of this orifice. Such regions of high positive potential are caused by an accumulation of low energy ions in a sea of relatively high-energy, ionizing electrons. Downstream of the region of high potential, both ions and electrons flow away from the contactor (ions being accelerated and electrons being decelerated) as they attempt to correct the imbalance that causes the region of high positive potential

to develop. It would appear that a contactor operating in this manner (emitting both ions and electrons) would be particularly well suited to general spacecraft charging control. This suitability is suggested because small changes in the potential difference between a spacecraft (and its contactor) and the ambient plasma would be expected to cause the current associated with the ions or electrons to be altered slightly. This would be expected in turn to facilitate the modest changes in current that would be required to prevent the spacecraft from becoming either substantially positive or negative of the ionospheric plasma in natural spacecraft charging situations.

In addition to the studies mentioned above, a section of this report concerns experiments focused on the selection of a plasma source that serves best to produce a simulated (or ambient) plasma for the conduct of ground-based plasma contactor tests. Early tests of plasma contactors were conducted under this grant using hot filaments to supply electrons into an ambient plasma [23]. These hot filaments exhibited substantial "space-charge" limitations not expected in space, that limited their rate of electron supply. They were, therefore, replaced with longer lifetime, high-current/low-voltage hollow cathode plasma sources. The hollow cathode simulator performed adequately as an ambient plasma generator, but several problems arose when plasma contactor tests were being performed. Specifically, ambient plasma densities changed when the electron emission current was varied, and Langmuir probe data were excessively noisy under some operating conditions (in some simulator electron emission current ranges these data could not be collected at all). In an effort to mitigate these

problems, various discharge chamber plasma sources were investigated as replacement simulated ambient plasma sources (simulators).

The mechanisms by which the simulator influences the ambient plasma conditions can be inferred from Fig. 1. The ambient plasma is sustained through 1) ionization of neutral atoms in the tank by electrons accelerated away from the simulator, 2) ionization of these same atoms by Maxwellian electrons in the ambient plasma and 3) ions supplied directly from the simulator and contactor discharges. In order to control the ambient plasma density (and possibly the ambient plasma electron temperature) to values closer to those observed in low Earth orbit, it is primarily the first of these processes that must be limited. In Fig. 1, the potential difference between the ambient plasma and the simulator cathode is labelled ΔV_S. Electrons coming from the simulator cathode and discharge chamber plasma that do not lose energy in collisions can reach the ambient plasma with a kinetic energy as great as ΔV_S (in eV). If ΔV_S is greater than the ionization threshold of the neutral atoms in the ambient plasma, these hot electrons can ionize them. Consequently, one can reduce the rate of ionization in the vacuum tank by reducing ΔV_S or by producing low energy electrons in a discharge chamber at a potential V_{SD} that is close to ΔV_S and then releasing them into the ambient plasma. Other considerations important in the selection of a simulator include 1) generation of a large, uniform ambient plasma region, and 2) creation of a relatively low noise ambient plasma.

APPARATUS AND PROCEDURE

In order to study the plasma contacting process, the apparatus shown schematically in Figs. 2 and 3 was constructed. Physically this apparatus consists of two plasma producing devices. One is shown at the right of each figure and is labeled "simulator". It is used to generate a simulated ionospheric plasma (the ambient plasma). The other device, shown on the left and labeled "contactor", is used to generate a contactor plasma plume. The contactor and the contactor plasma plume are biased relative to the ambient plasma to induce current flow. Also shown are the power supplies and instrumentation needed to sustain and measure the characteristics of the plasmas produced. The simulator and contactor devices are separated by 2.7 m and are located within a 1.2 m dia. by 5.3 m long vacuum chamber. The contactor utilizes a hollow cathode with a 6.4 mm dia. orifice plate and an electron emitting insert. The insert used in this cathode was fabricated by rolling 0.013 mm thick tantalum foil into the shape of a hollow cylinder and treating it with Chemical R-500 (a double carbonate [$BaCO_3$, $SrCO_3$] low work function mixture that has been made by J.T. Baker Co. but is no longer in production). The insert was then placed inside the 6.4 mm dia hollow cathode tube. The orifice in the contactor orifice plate is 0.76 mm in diameter. The contactor anode is a 12 cm dia stainless steel plate with a 1 cm dia. tantalum insert having a 5 mm dia. orifice in it. The anode plate and the tantalum anode insert are located concentric with the hollow cathode centerline on a plane ~2 mm downstream of the cathode orifice plate. The simulator device was changed several times over the course of this experimental investigation into configurations that will be described.

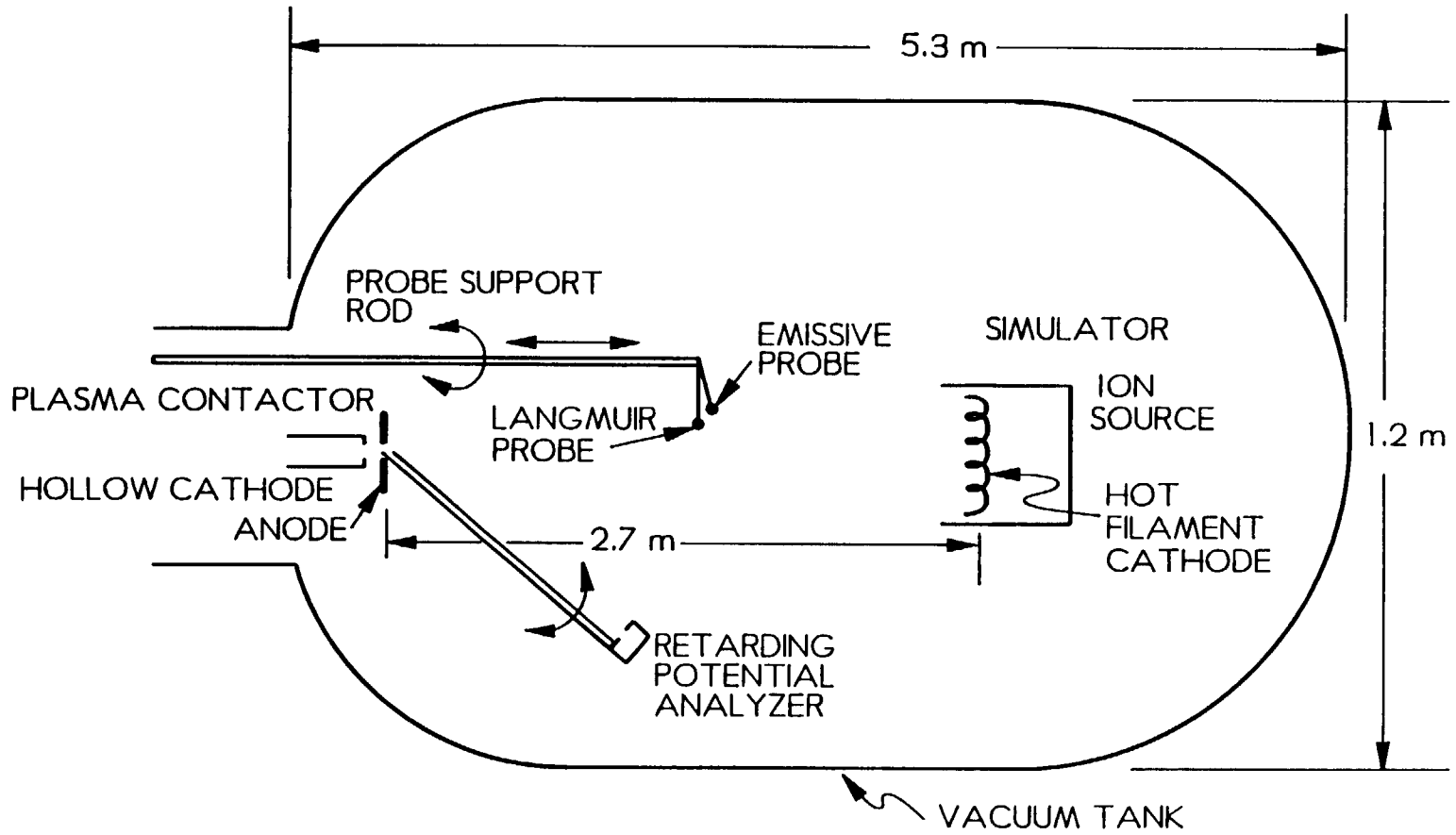

Fig. 2 Experimental Apparatus

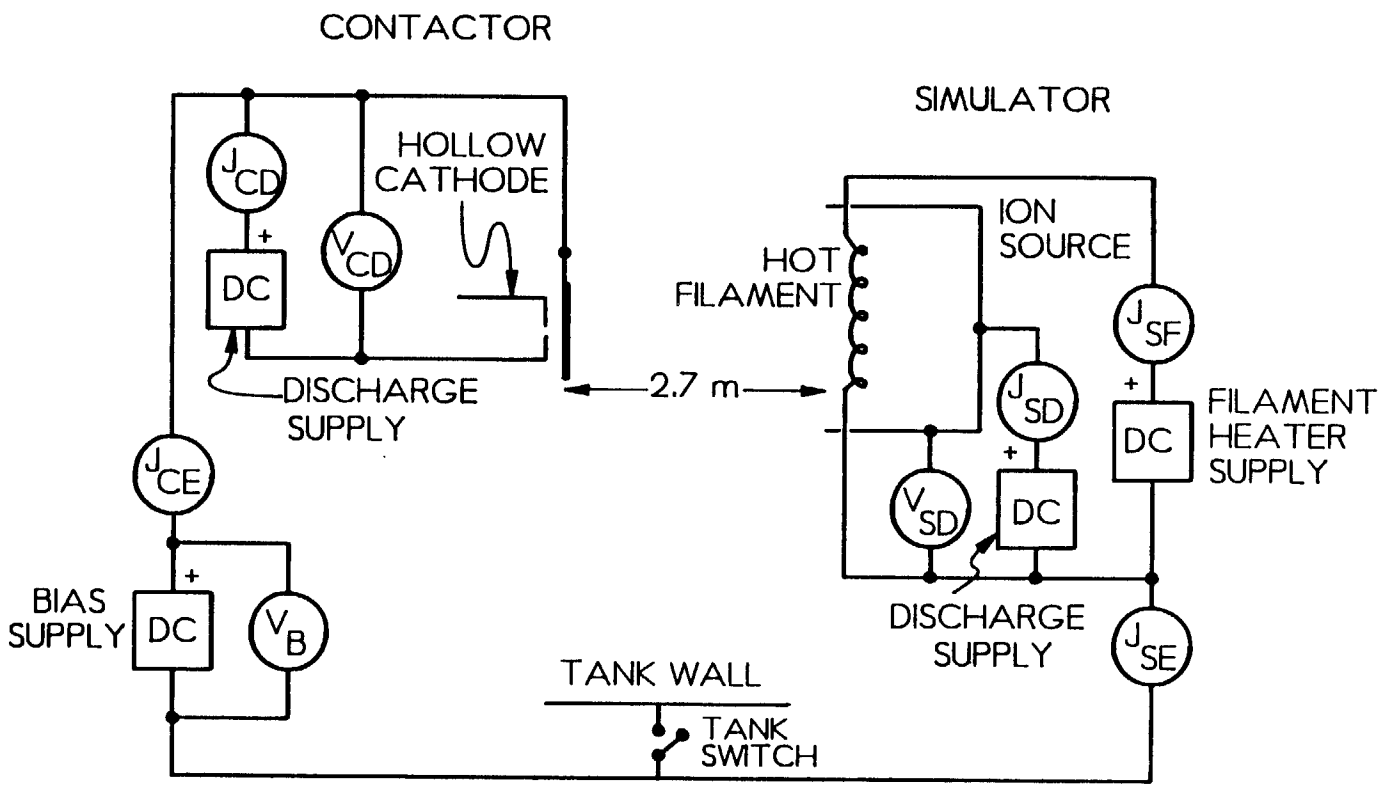

Fig. 3 Electrical Schematic

Typical tests were conducted by heating the contactor hollow cathode to a temperature where significant thermionic electron emission could occur from its insert (~1300 K), establishing a high expellant (xenon) flowrate through it, and biasing its anode positive using the discharge supply to initiate a cathode-to-anode discharge. The simulator plasma device was also started in a similar manner. Next, the desired contactor and simulator flowrates and discharge current levels were established; the contactor was biased relative to the simulator using the bias power supply; and voltage, current and probing instrument data were collected. The voltages and currents measured during typical tests are designated by the symbols shown within the circles in Fig. 3; they include the contactor and simulator discharge currents and voltages (J_{CD}, J_{SD}, V_{CD} and V_{SD}), the bias voltage (V_B) between the contactor and simulator, and the contactor and simulator electron emission currents (J_{CE} and J_{SE}).

The tank bias switch shown in Fig. 3 was installed so the vacuum tank could be allowed to float relative to the contactor-simulator system or be connected to the simulator. This was done so the effects of relative tank bias on the plasma contacting process could be investigated.

The plasma environment produced between the contactor and the simulator was probed using the various instruments shown in Fig. 2. They include an emissive probe [24], a Langmuir probe [25,22], and a retarding potential analyzer (RPA) [20]. The RPA used in the study is shown in more detail in Fig. 4. It consists of a cylindrical Faraday cage with an orifice plate at one end -- the orifice hole dia of 3 mm was selected to be smaller than the typical ambient plasma Debye length.

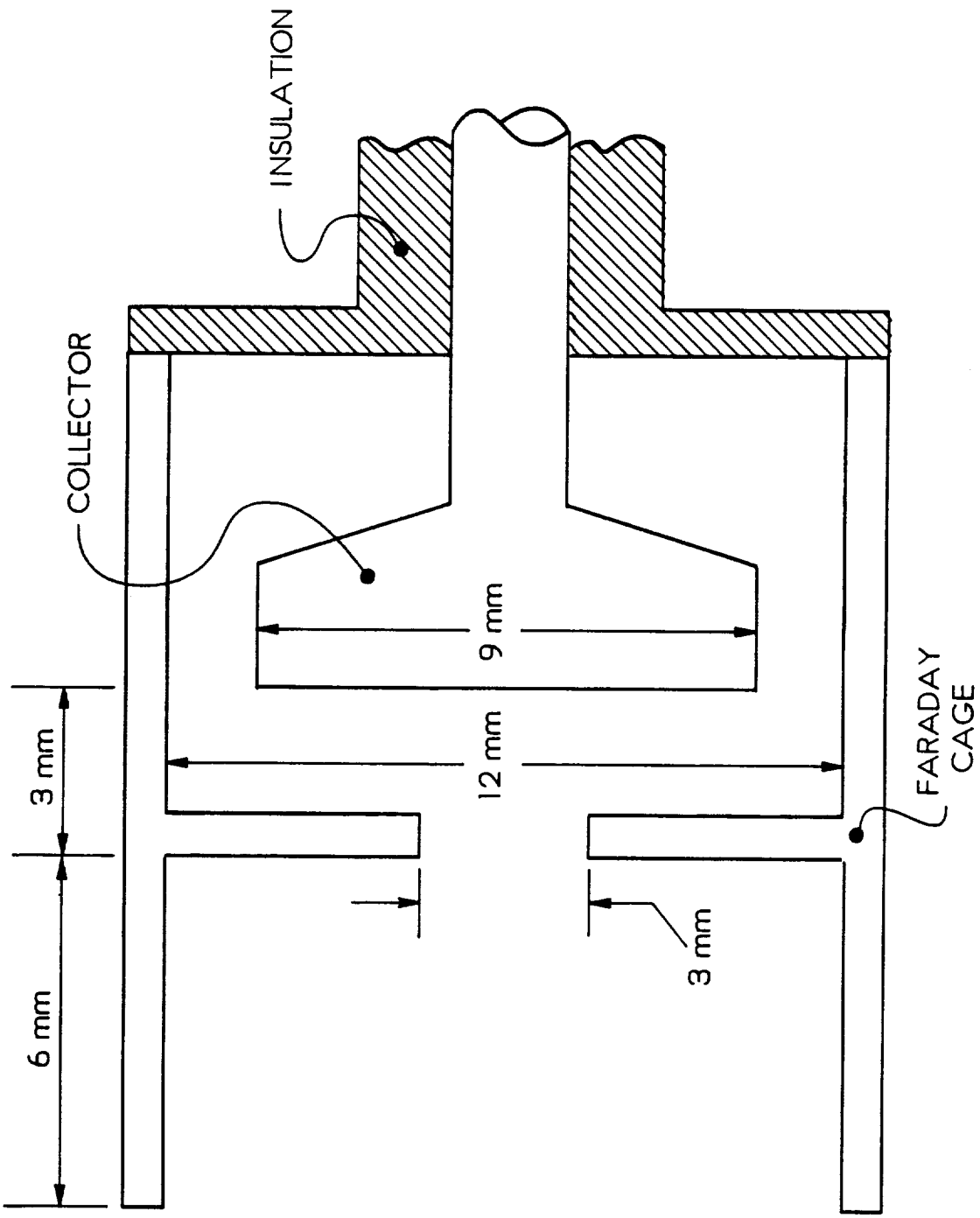

Fig. 4 Retarding Potential Analyzer

The RPA was generally positioned about 18 cm downstream of the contactor on the centerline of the vacuum tank. The Faraday cage was typically held at 40 to 60 V negative of the plasma in which it was immersed. This negative bias shields the ion collector electrode inside the Faraday cage. The probe is operated by first sighting the RPA orifice at the plasma contactor, and then sweeping the voltage of the collector from -10 to +80 V (measured with respect to the contactor cathode or some other convenient reference in the circuit) and recording the ion current flowing to the collector surface. The actual details of the current/voltage traces obtained are discussed in the results section.

As mentioned previously, several different devices were used for the simulator. The goal of these experiments was to find a suitable plasma source which would produce 1) a large, uniform, relatively quiescent ambient plasma region and 2) an ambient plasma with a low density and a low electron temperature. The plasma source devices which were investigated are shown in Figs. 5 and 6. Because they are all modifications of ring-cusp discharge chambers which are typically used as ion sources in ion thruster applications [26], they resemble one another physically.. Plasma is generated in the sources by collisions between high energy discharge electrons and neutral atoms. In order to increase the efficiency of this process, magnetic fields are used to protect anode surfaces and chamber walls from direct loss of discharge electrons. The magnetic field used in the ion sources is shaped in a ring-cusp geometry by small (1 cm x 1 cm x 0.5 cm) samarium cobalt permanent magnets. In order to ensure the good coupling between the plasma in the source and the expanding plasma region, the devices were operated without plasma extraction grids.

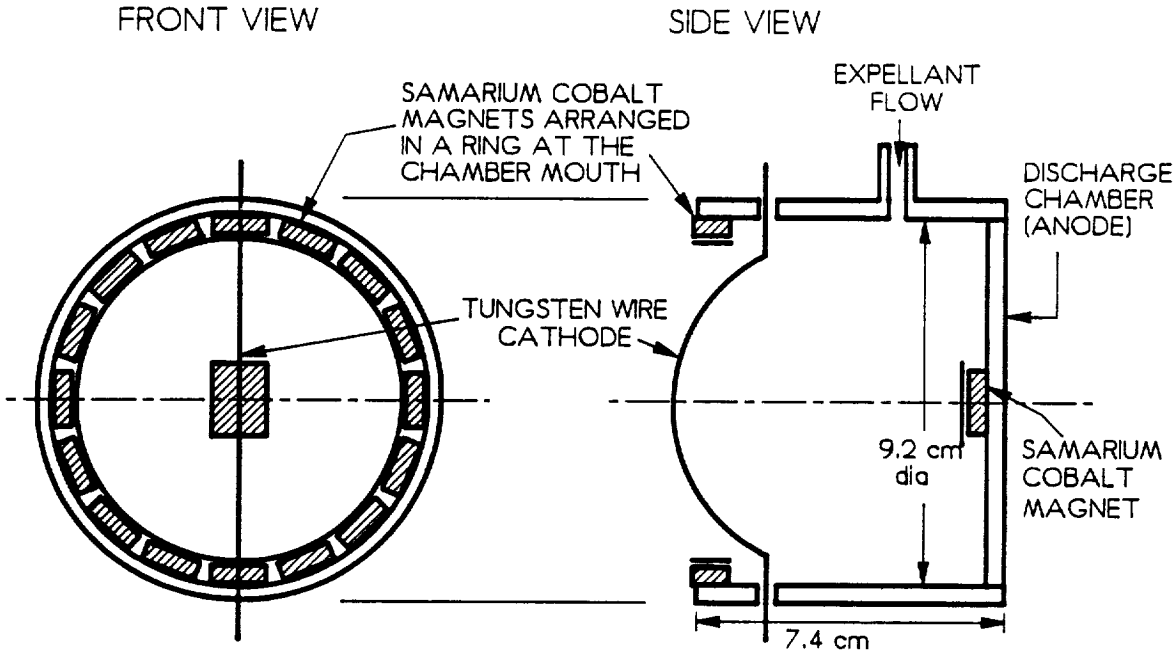

a. DIAGONAL FILAMENT CATHODE

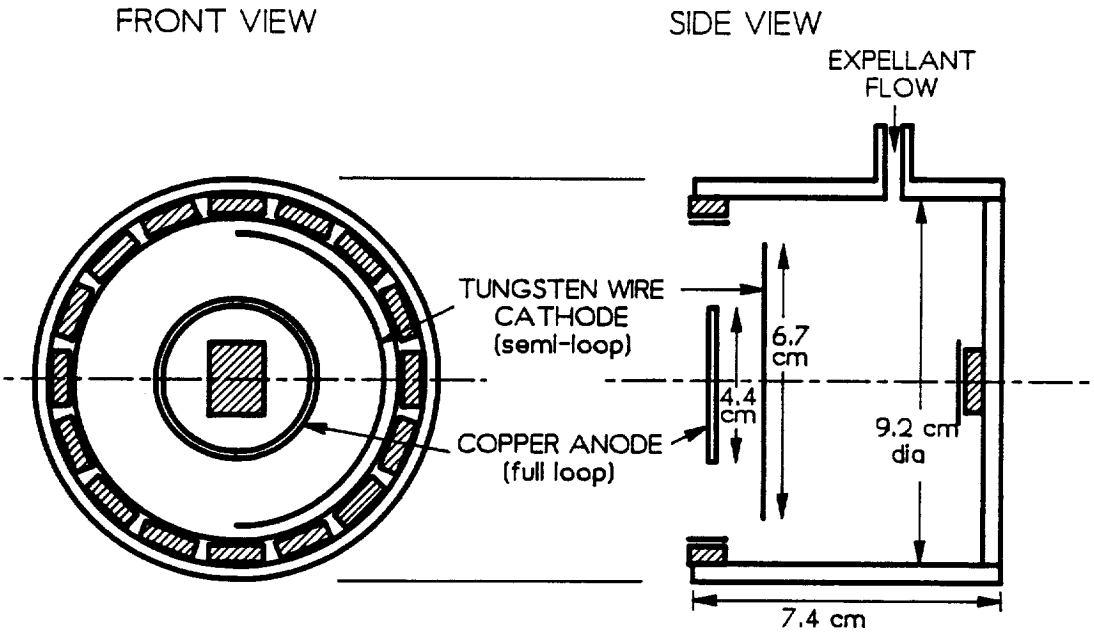

b. SEMI-LOOP FILAMENT CATHODE

Fig. 5 Hot Filament-Based Discharge Chambers Used to Produce Ambient Plasma

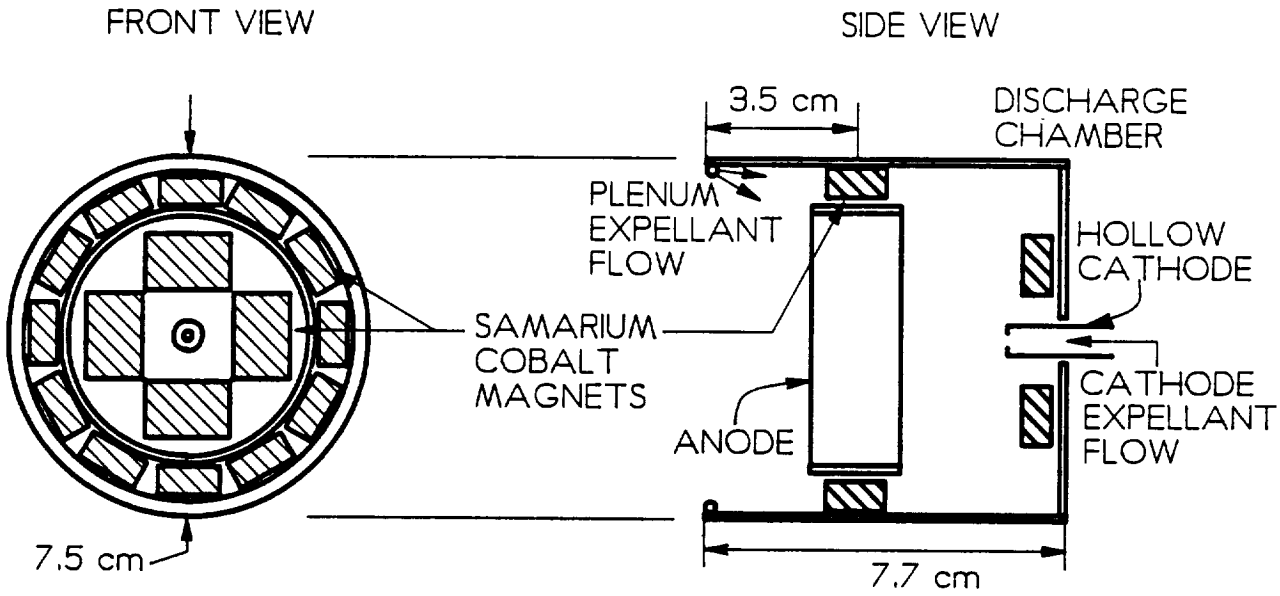

a. HOLLOW CATHODE AT BACK WALL

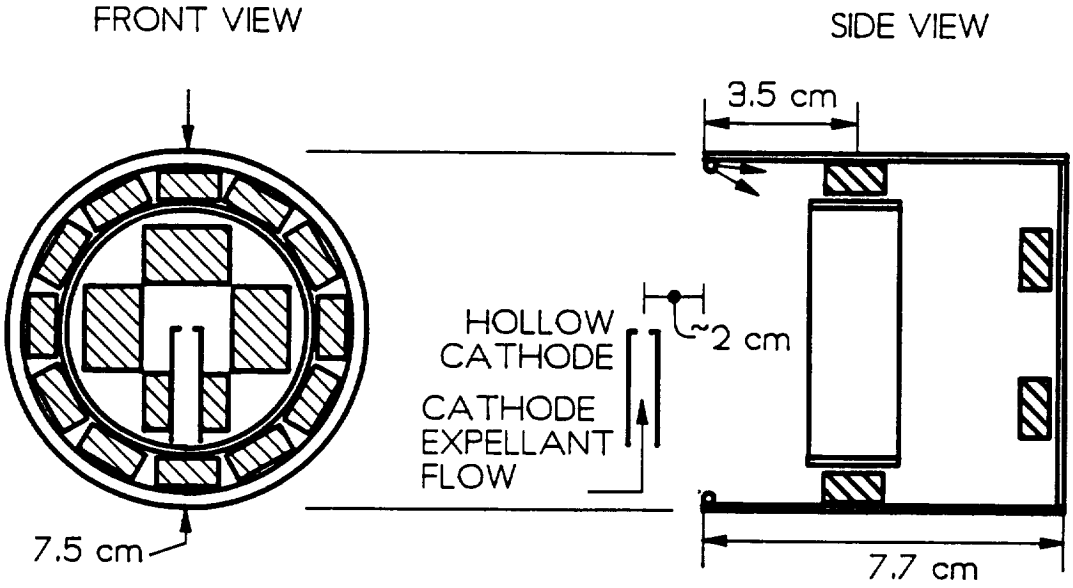

b. HOLLOW CATHODE AT CHAMBER MOUTH

Fig. 6 Hollow Cathode-Based Discharge Chambers Used to Produce Ambient Plasma

The main differences between the devices are reflected in their electrode designs. For example, Fig. 5a contains a ring-cusp source which is equipped with a tungsten wire cathode. The wire cathode was stretched diagonally across the mouth of the chamber and when heated to thermionic temperatures it emitted electrons to the ambient plasma and the discharge chamber body (which served as the anode for this device). Figure 5b shows a source equipped with a semi-loop wire cathode and a copper loop anode which are oriented circumferentially. The discharge chamber body of this device could also be held at anode potential or be allowed to float. The ring-cusp sources shown in Figs. 6a and 6b use hollow cathodes to supply the discharge and emission currents. The hollow cathode orifice is located near the back wall of the device shown in Fig. 6a and on the centerline at the mouth of the device shown in Fig. 6b.

The devices shown in Figs. 5 and 6 were connected electrically as shown in Figs. 7 and 8. The electrical configurations resemble the physical shape of the devices and are numbered from 1 to 5. Simulator configurations No. 1 and No. 2 are actually the same hot filament-based device, but No. 2 utilizes the discharge chamber body as an additional anode surface. Simulator No. 3 is the diagonal hot filament-based source, and Simulator Nos. 4 and 5 are the hollow cathode-based devices. The details of the operation of these devices are included in the Results section of the report.

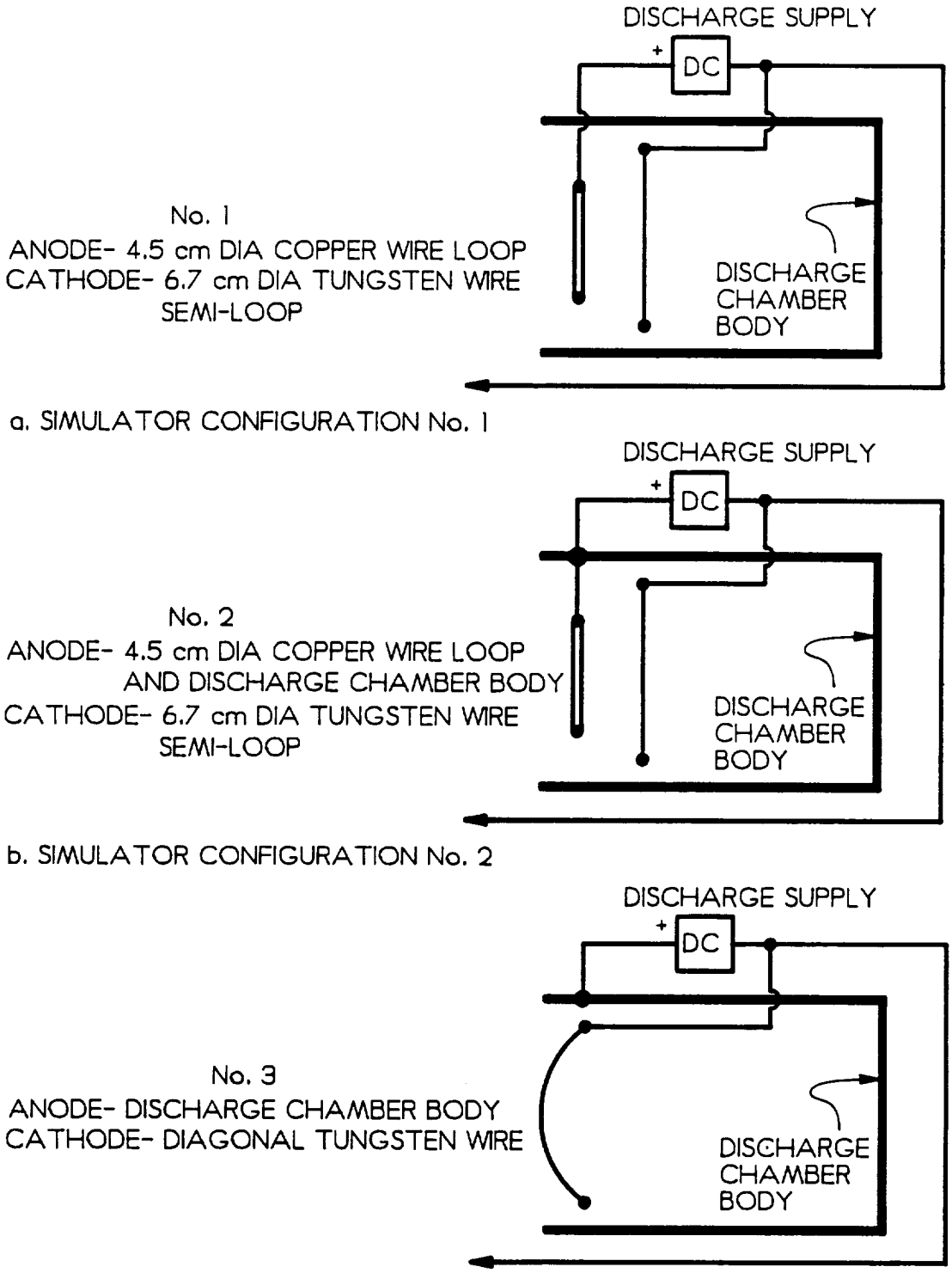

Fig. 7 Test Configurations for Hot Filament-Based Discharge Chamber Simulators

No. 4

ANODE- FLAT COPPER LOOP AND
DISCHARGE CHAMBER BODY
CATHODE- HOLLOW CATHODE

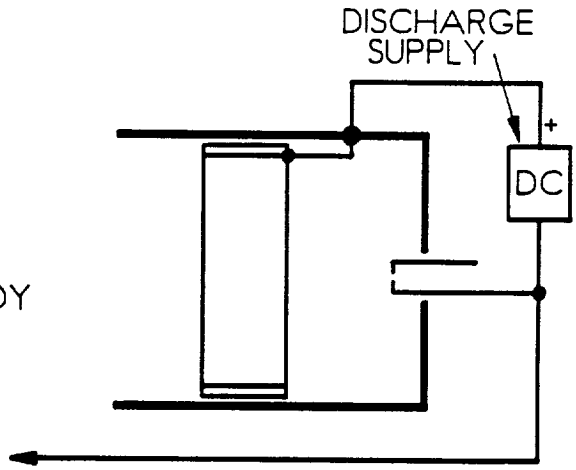

a. SIMULATOR CONFIGURATION No. 4

No. 5

ANODE- FLAT COPPER LOOP
CATHODE- HOLLOW CATHODE

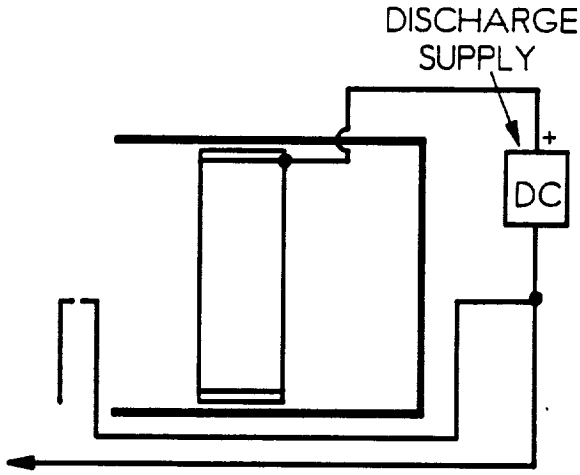

b. SIMULATOR CONFIGURATION No. 5

Fig. 8 Test Configurations for Hollow Cathode-Based Discharge Chamber Simulators

RESULTS

High Electron Collection Current Experiments

Previous experimental work performed under this grant on plasma contactors has been carried out at electron collection current levels below 1 A. At these low current levels, a relatively simple model of the electron collection process gives good agreement with experimental results [16]. The model is based on the assumption that separable phenomena occur in three different regions. The boundary of the first region (at the downstream edge of the contactor plasma plume) is located so that the ion current emitted from it satisfies the ion current demanded by the double layer. This current is given as the product of the surface area of the region and the Bohm current density associated with the ions contained within it. The second region (the contactor double layer) supports most of the potential difference between the contactor plasma plume and is described by the equations for a spherical of spherical sector double layer. Both the ion current being emitted from the plasma plume and the electron current being collected from the ambient plasma are assumed to flow through this double layer at their space-charge limited values. The third region is the ambient plasma and the electron current collected from it is given in the model as the product of the random electron current density and the surface area of the interface between the double layer and the ambient plasma.

Experiments conducted at NASA Lewis Research Center on various hollow cathode-based plasma contactors including one built and tested at Colorado State suggested that the simple model works at low electron collection currents (under 1 A), but at higher current levels it begins to break down [1,2]. In order to determine if this would occur in the

Colorado State facility, the power supply used to bias the contactor relative to the simulator was replaced by one with a higher current and voltage capability. This section will discuss typical results obtained at electron collection currents up to ~3 A and the procedures used to operate at these higher currents.

An electrical schematic of the experimental apparatus is shown in Fig. 3. The simulator used for the experiments described in this section is shown in Fig. 5b and electrically connected as shown in Fig. 7a -- Simulator No. 1. The discharge chamber simulator was operated at a discharge current (J_{SD}) and voltage (V_{SD}) of 50 mA and 40 V, respectively. The tank switch shown in Fig. 3 was used in these tests to float or ground the contactor and simulator circuit to the vacuum tank. At several operating conditions the plasma properties were probed with emissive and Langmuir probes and the system operating conditions associated with the symbols listed within the circles of Fig. 3 were recorded.

The plasma properties measured along the tank centerline in an experiment for which the tank was floated and then grounded are compared in Fig. 9. The electron collection current flowing to the contactor remained constant at 700 mA for both cases and the contactor was operated at the conditions listed in the legend. The top plot shows how the plasma potential varies downstream of the contactor. The features of the potential profile include a contactor double layer located at about 10 cm and an intermediate double layer at about 35 to 65 cm for both curves. Except for the uniform vertical offset in potential, the curves are considered to agree within the limits of experimental error (± 1 V). Corresponding axial profiles of plasma density (n_e) and

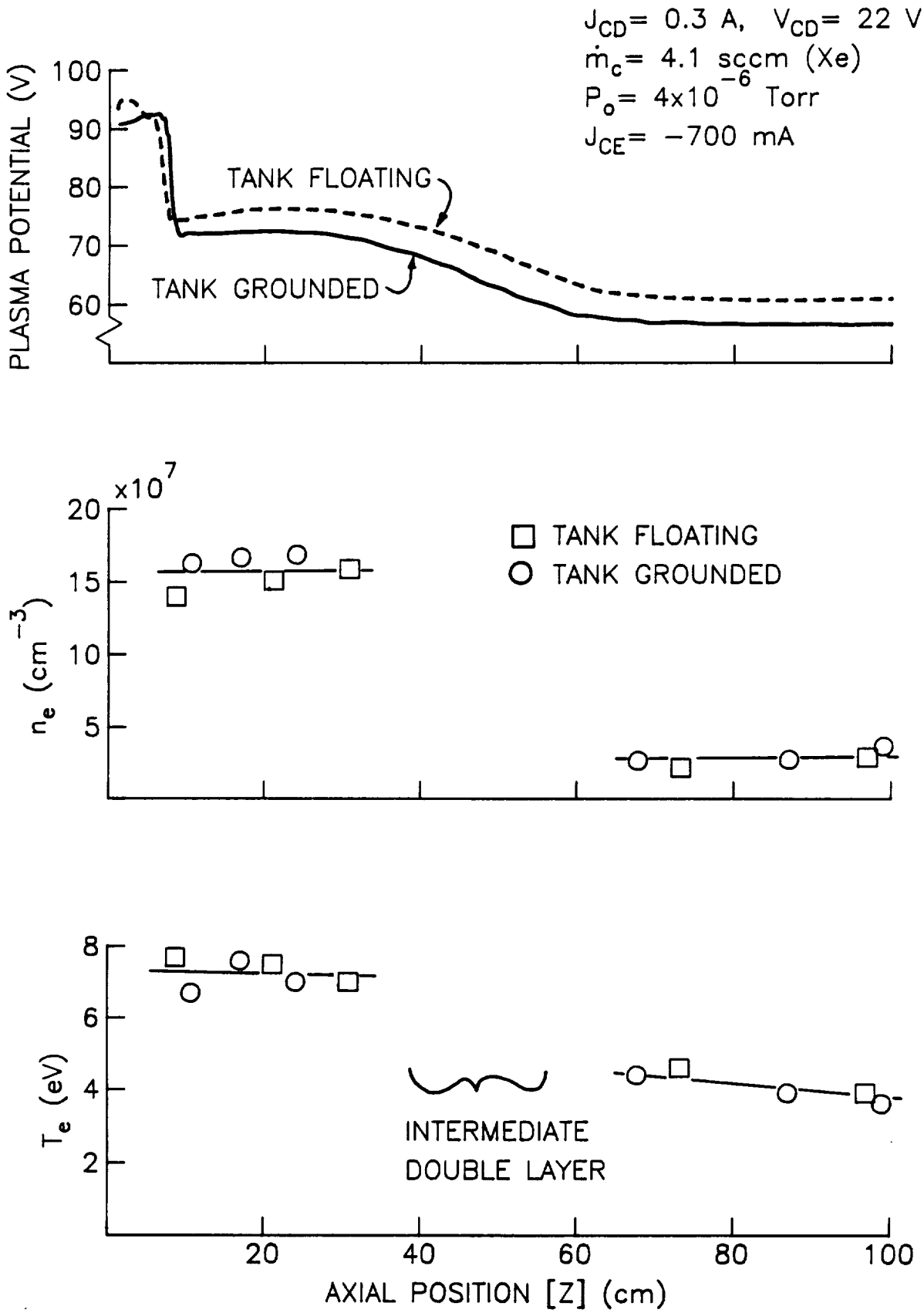

Fig. 9 Comparison of Plasma Properties with Floating and Grounded Vacuum Tank

electron temperature (T_e) are also shown in Fig. 9. The precision of plasma density and electron temperature data were ± 25 % and ± 15 %, respectively. Thus the data in Fig. 9 agree within the limits of experimental error. However, the absolute magnitude of the true electron density could differ from the measured density by more than the indicated precision because of a systematic error related, for example, to the plasma noise level. In conclusion, the data in Fig. 9 suggest that the results are not affected significantly by changes in vacuum tank potential over the grounded-to-floating range.

An interesting feature of the middle and bottom plots of Fig. 9 is the large change in plasma properties observed across the intermediate double layer. From the low potential boundary to the high potential boundary of the intermediate double layer, the plasma density increases by a factor of five (from 2.7 to 15 x10^7 cm^{-3}) and the electron temperature increases by a factor of two (3.5 to 7 eV). Similar results have been reported by Vannaroni, et. al, except they report generally lower electron temperatures in their experiment [5]. As mentioned in the introduction, the phenomena that cause the intermediate double layer are not understood by us. However, it is noted that the intermediate double layer seems to be affected more by the magnitude of the electron collection current and the simulator operating conditions than by the contactor operating conditions.

Figure 10 compares the plasma potential profile measured at an electron collection current of 2.7 A to one measured at a lower value of 700 mA. The structures are similar on both curves; this suggests that the basic phenomena described in the model for low electron currents

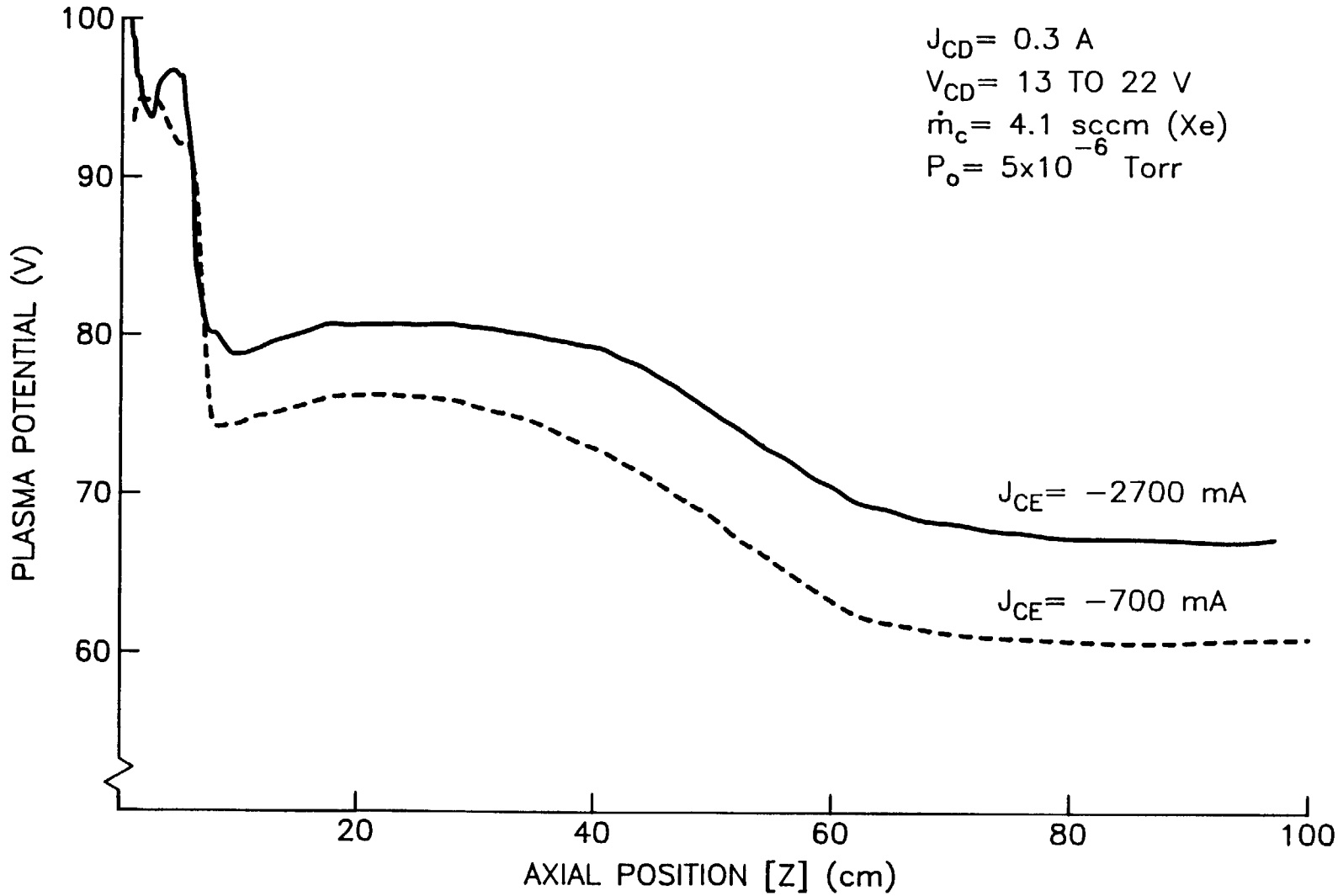

Fig. 10 Comparison of Plasma Potential Profiles Obtained at High and Low Electron Collection Current Levels

probably applies at higher currents. This degree of experimental correlation was not observed in the NASA Lewis tests [1,2] possibly because of 1) the lower neutral pressures in the Lewis facility (50% of those at CSU) and 2) different and more severe interactions between the contactor and intermediate double layers that were observed in the Lewis tests. Figure 11 presents contactor performance data collected over a range of relatively high electron collection currents. It is a plot of contactor potential (the potential difference between the contactor anode and the ambient plasma -- see Fig. 1) versus electron collection current. The contactor potential data are shown to scatter around 30 to 35 V for currents up to 2.7 A. No data could be obtained at currents greater than 2.7 A because large "space-charge" limitations developed at the simulator filament cathode which precluded emission of greater currents without excessive voltage drops.

Effects of Operating Parameters on Electron Emission Phenomena

A great deal of understanding of the process of electron emission from a hollow cathode-based plasma contactor to an ambient plasma can be obtained from plasma potential profiles like the one shown in Fig. 12. In this case the contactor cathode, at zero potential and zero axial position, is emitting 61 mA of electrons into an ambient background plasma located about 1 m downstream of the contactor. A noteworthy feature of this plasma potential profile is the potential hill structure that develops immediately downstream of the contactor. It is postulated that this unusual potential hill develops as a result of a high rate of atom ionization at the location of the hill. Because the contactor is emitting both neutrals and electrons (both have high densities near the contactor), a high ionization rate can develop. Under this condition,

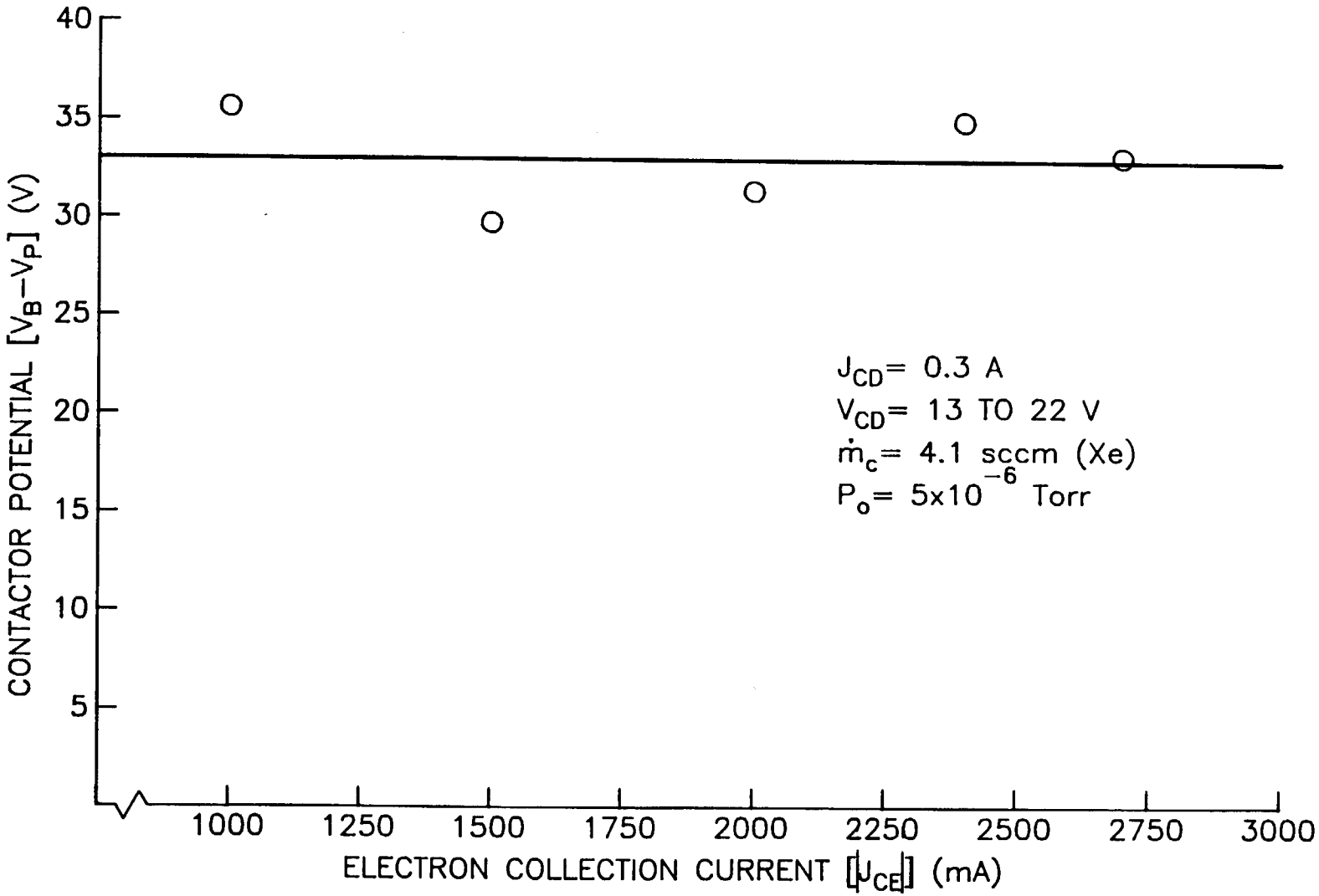

Fig. 11 Plasma Contactor Characteristic Curve at High Election Collection Current Levels

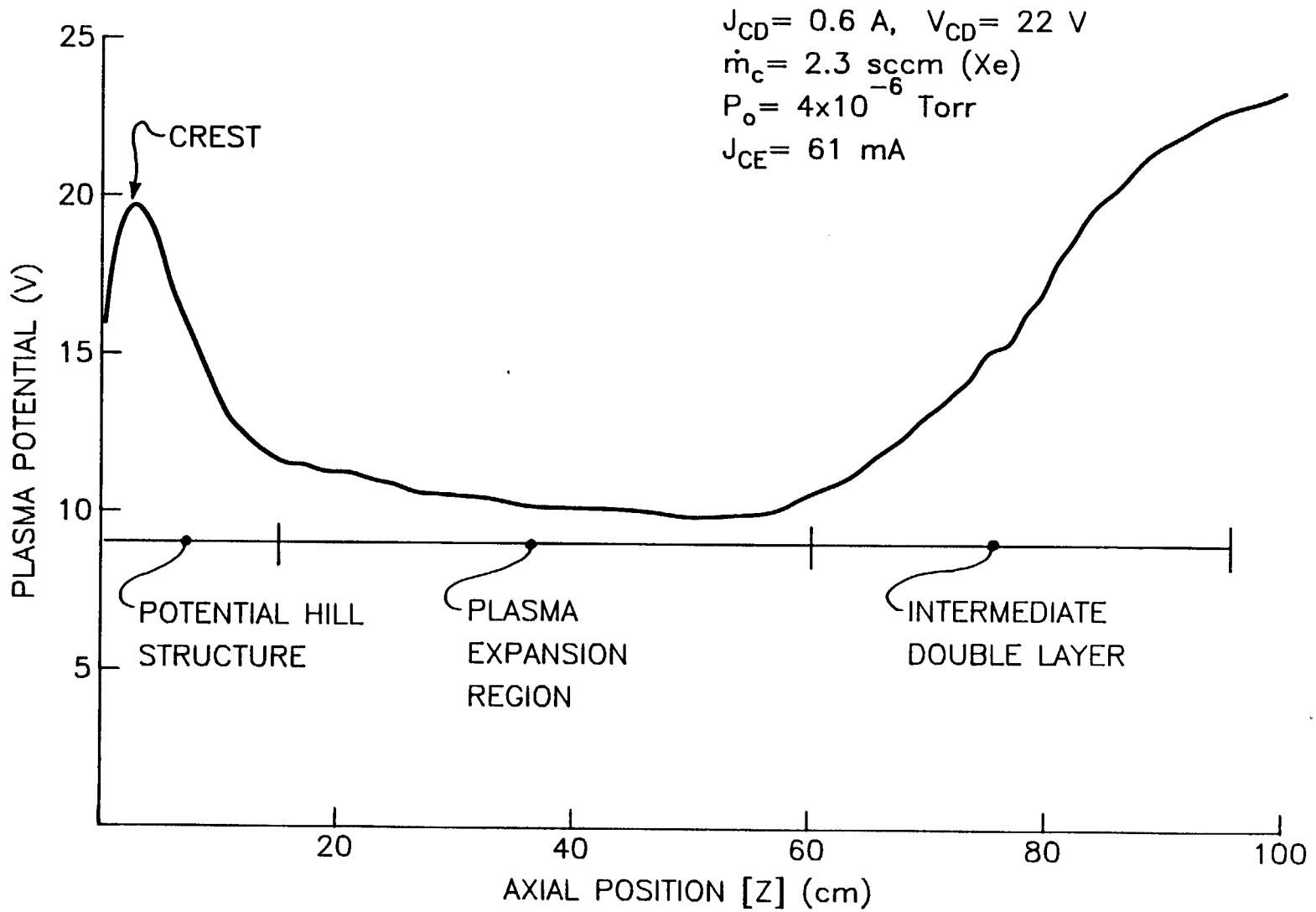

Fig. 12 Plasma Potential Profile: Contactor Emitting Electrons

electrons that induce ionization would still be expected to have substantial kinetic energies after an ionization event, and they would therefore be expected to leave the hill region quickly. However, the more massive ions would be left behind. These ions would be expected to induce the positive space-charge density that causes the hill to develop. The crest potential might be expected to rise until electric field forces were sufficient to decelerate the electrons and accelerate the ions out of the region of the potential hill at rates limited by a basic physical constraint such as energy conservation.

The data shown in Fig. 12 were obtained using an emissive probe to record the plasma potential. It is known that floating emissive probes indicate potentials that fall progressively further below true plasma potential as they are moved into higher density plasmas [24]. Because plasma density increases with decreasing distance from the hollow cathode, it is considered likely that the true potential at the crest of the hill is substantially higher and at a different position than the measured one shown in Fig. 12.

Downstream of the potential hill, the plasma potential is relatively uniform (from 15 to 60 cm), but the plasma density decays as $1/r^2$ thereby suggesting a region of radial plasma expansion. This plasma density decay ends at about 60 cm where the potential rises. This region of changing potential (60 to 100 cm) is termed the intermediate double layer. Langmuir probe data have shown that it separates the region of plasma expansion located just downstream of the potential hill from the ambient plasma that fills the majority of the vacuum test facility [16]. It is suggested therefore that the

intermediate double layer develops to accommodate boundary condition matching between the expanding and ambient plasmas.

Electron emission experiments are conducted by first starting and stabilizing the discharges associated with the contactor and simulator devices. Note that for contactor electron emission tests, a simulator was needed to generate plasma and collect electrons emitted by the contactor. The simulator device used for these tests was a simple hollow cathode device equipped with a 3 cm tantalum anode that was operated at a discharge current of 1 A and a flowrate of 3.3 sccm (Xe). The electrical connections between the bias supply, contactor, simulator and tank were made so that most of the electrons emitted from the contactor would be collected by the simulator rather than the tank. In order to accomplish this, the tank was connected to the contactor cathode and the negative terminal of the bias supply. Typical tests were initiated by adjusting the potential difference between the contactor cathode and the simulator anode (and therefore the ambient plasma) using the bias supply (V_B) in order to draw the desired electron emission current (J_{CE}) from the contactor. Next, the plasma potential structure downstream of the contactor was measured using the emissive probe and finally, the energy/current density characteristics of the ions flowing from the potential hill structure away from the contactor were measured using the retarding potential analyzer (RPA).

In order to investigate the potential hill structure and the processes that were occurring, the RPA was placed 17.7 cm downstream of the contactor (on the contactor/vacuum tank centerline) and sighted at the contactor orifice. Typical RPA data collected using the probe are shown in Fig. 13. The top plot shows ion current density to the RPA

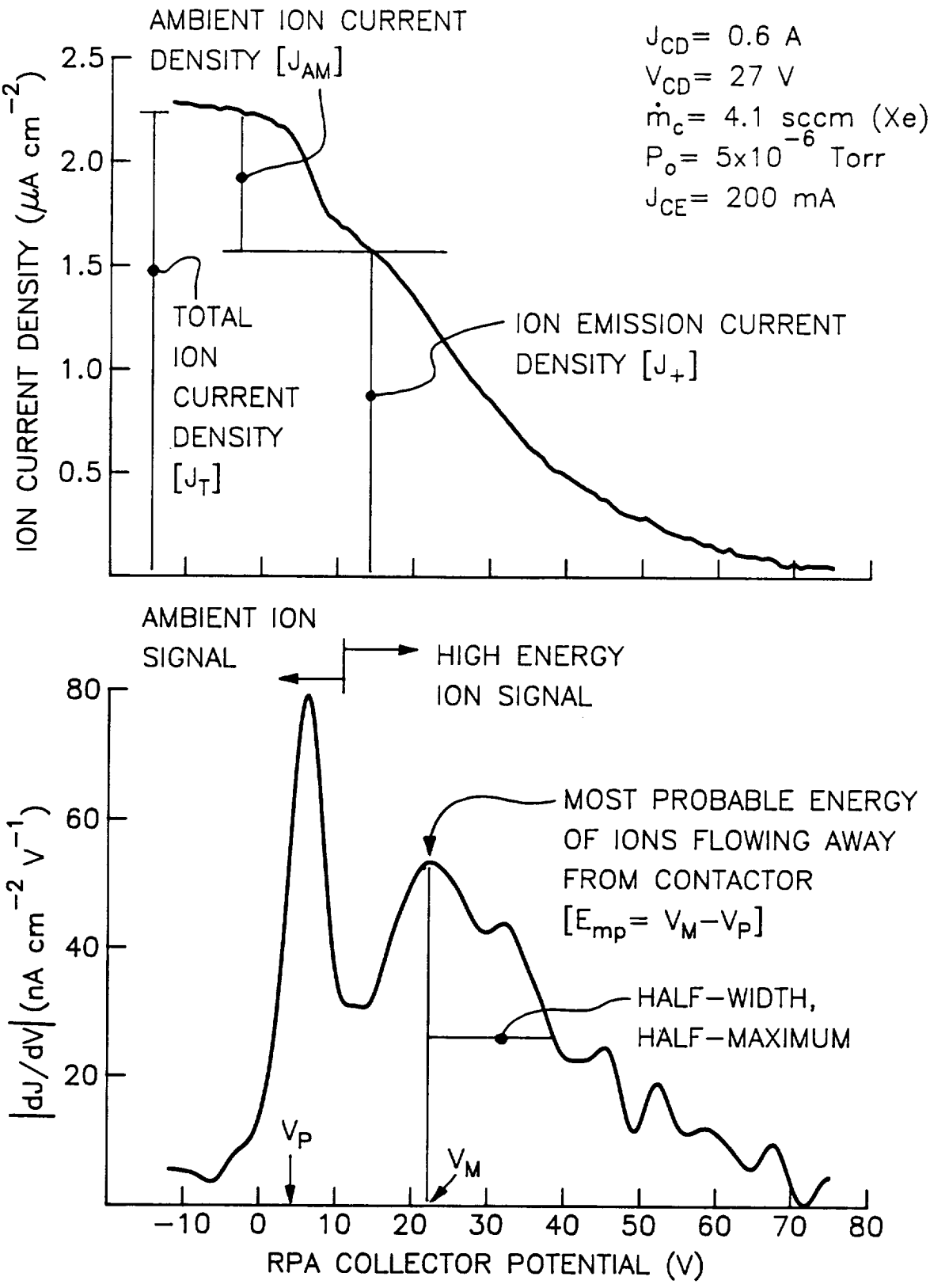

Fig. 13 Typical RPA Data: Contactor Emitting Electrons

collector versus the collector potential measured with respect to the contactor cathode and the vacuum tank. It shows the ion current to the RPA collector decreases as the potential applied to it is increased. Hence, ambient ions in the vicinity of the probe, which have the lowest energies, are repelled at the lowest collector potentials. The current density of these ambient ions is labelled J_{AM} in Fig. 13. It is defined as the current density measured at low voltage (at ~ 0 V) minus the current density measured at the plasma potential sensed by the emissive probe positioned near the RPA location (in the case of the data shown in Fig. 13 this plasma potential was 16.2 V).

Plasma potential can also be determined approximately by finding the RPA collector potential where the derivative of RPA collector current with collector potential is a maximum. This value of plasma potential (V_p) is identified on the lower plot in Fig. 13. It was found to be about 5 to 10 V below the plasma potential indicated by the emissive probe. This relatively large degree of error could be due to 1) a resistive layer building up on the RPA collector, 2) poor collimation characteristics of the RPA Faraday cage or 3) plasma potential fluctuations which alternatively drive the RPA collector potential into the ion acceleration/ion deceleration regime and "round off" the ambient ion signal edge. At potentials several volts above the RPA plasma potential, only ions with high energies can reach the probe. The ion current density measured at plasma potential is termed the ion emission current density, J_+. As shown on Fig. 13, the sum of the ambient and ion emission current densities is the total ion current density J_T.

The lower plot in Fig. 13 shows the absolute value of the derivative of the upper plot. This derivative facilitates discrimination between the ambient and high energy ions and enables one to obtain the ion energy distribution at the location of the RPA [8,20]. The ambient ions have a temperature of about 0.1 eV (even though the ambient ions will exhibit directed velocities at the RPA sheath edge determined by the ambient electron temperature). Consequently, most of the ambient signal shown in Fig. 13 occurs at RPA collector potentials near or below the plasma potential at the RPA, while the high energy ion signal is typically above plasma potential. The high energy ion signal is characterized here by two quantities; namely, the most probable ion energy (i.e. the ion energy corresponding to the maximum of the high energy signal -- $E_{mp} = V_m - V_p$), and the half width, half maximum energy spread ($\Delta E \approx 17$ eV in Fig. 13). In addition to the values of E_{mp} and ΔE the RPA data also indicate the maximum energy of the ions being emitted by the contactor (i.e. the RPA collector potential where the ion current density approaches zero minus plasma potential ≈ 60 eV in Fig. 13). This maximum energy can then be used to infer the maximum potential at the crest of the potential hill.

Figure 14 contains data obtained from many RPA traces like the one shown in Fig. 13. The upper plot in Fig. 14 displays the variation of ion emission current density (J_+) measured at the RPA location as a function of contactor discharge current (J_{CD}) for electron emission currents (J_{CE}) of 150, 250 and 500 mA. The ion emission current density is shown to increase linearly with the contactor discharge current. The bottom plot in Fig. 14 displays the ion emission current density/total ion current density ratio (J_+/J_T) as a function of contactor discharge

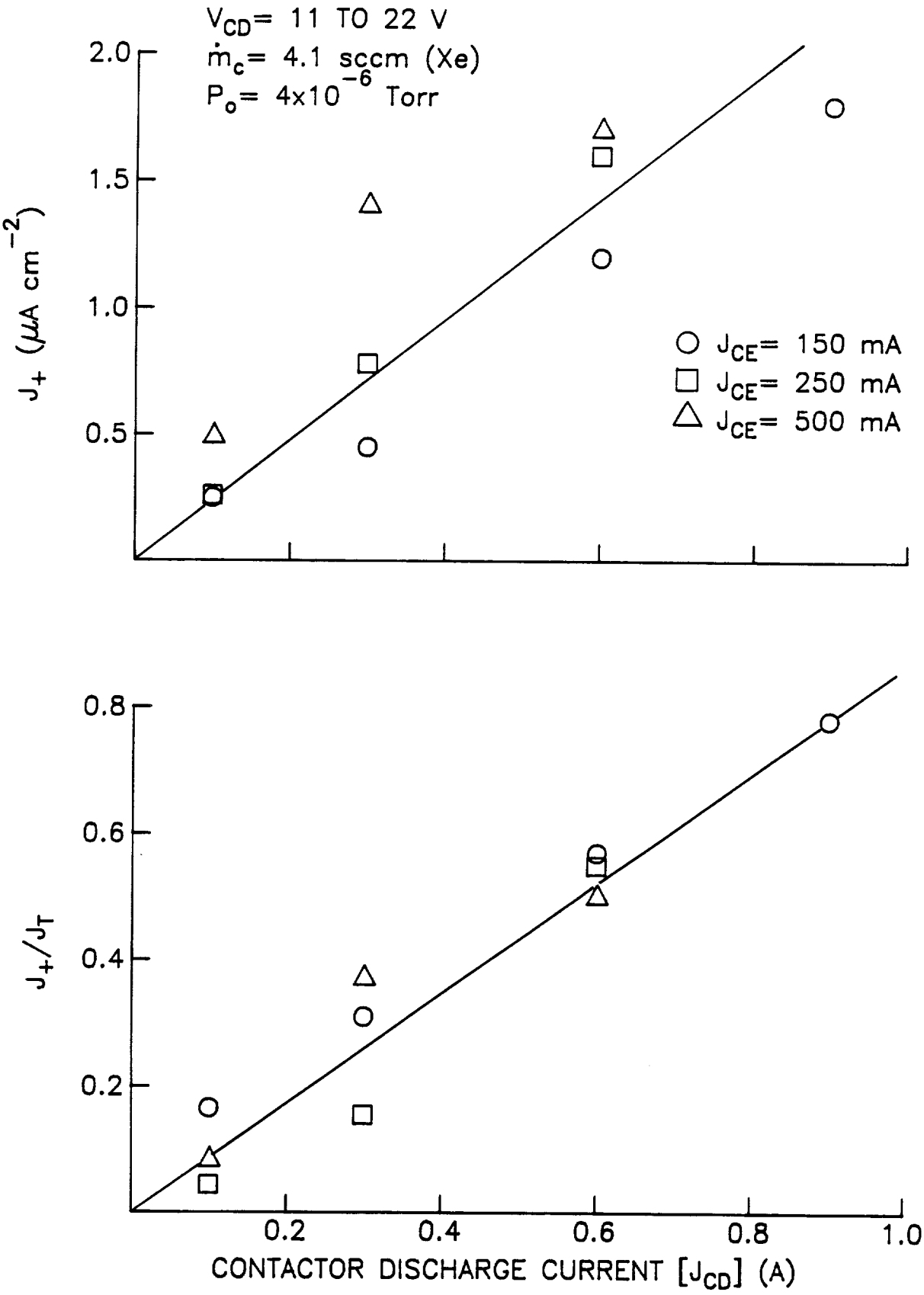

Fig. 14 Effects of Discharge Current and Electron Emission Current on Ions Emitted from the Potential Hill

and emission current. Similar to the upper plot, J_+/J_T increases with increasing discharge current. Considering the data from both plots, one can see that the total ion current density sensed at the RPA location remains relatively constant while the ion emission current density increases with contactor discharge current. Referring to Fig. 13 and then reconsidering Fig. 14, one can also conclude that the ambient ion signal (J_{AM}) must be decreasing slowly with increasing contactor discharge current. This test was considered to be preliminary and most probable ion energy (E_{mp}) and energy spread (ΔE) data were not collected, and, although Fig. 14 contains some information on the effects of electron emission current (J_{CE}), no clear conclusions can be drawn. Consequently, a more detailed experiment was conducted in which the contactor discharge was held constant and the electron emission current was varied.

Figure 15 shows the effects of electron emission current on ion emission current density (J_+), the ratio of ion emission-to-total ion current densities (J_+/J_T) and the most probable energy of the emitted ions (E_{mp}). The upper plot in Fig. 15 shows that the ion emission current density remains between 1.5 and 1.8 μA cm^{-2} as the electron emission current (J_{CE}) is increased from 20 mA to 1000 mA. However, the ratio of the ion emission-to-total current densities (J_+/J_T) decreases with increasing J_{CE} (see middle plot on Fig. 15). This trend indicates that the ions flowing from the potential hill region (J_+) dominate the ambient ion signal when J_{CE} is small but not when it is large and that J_{AM} increases with J_{CE}. In addition, E_{mp} is shown to decrease with increasing electron emission current. This trend suggests that the ion energy is higher for small electron emission currents. Data not

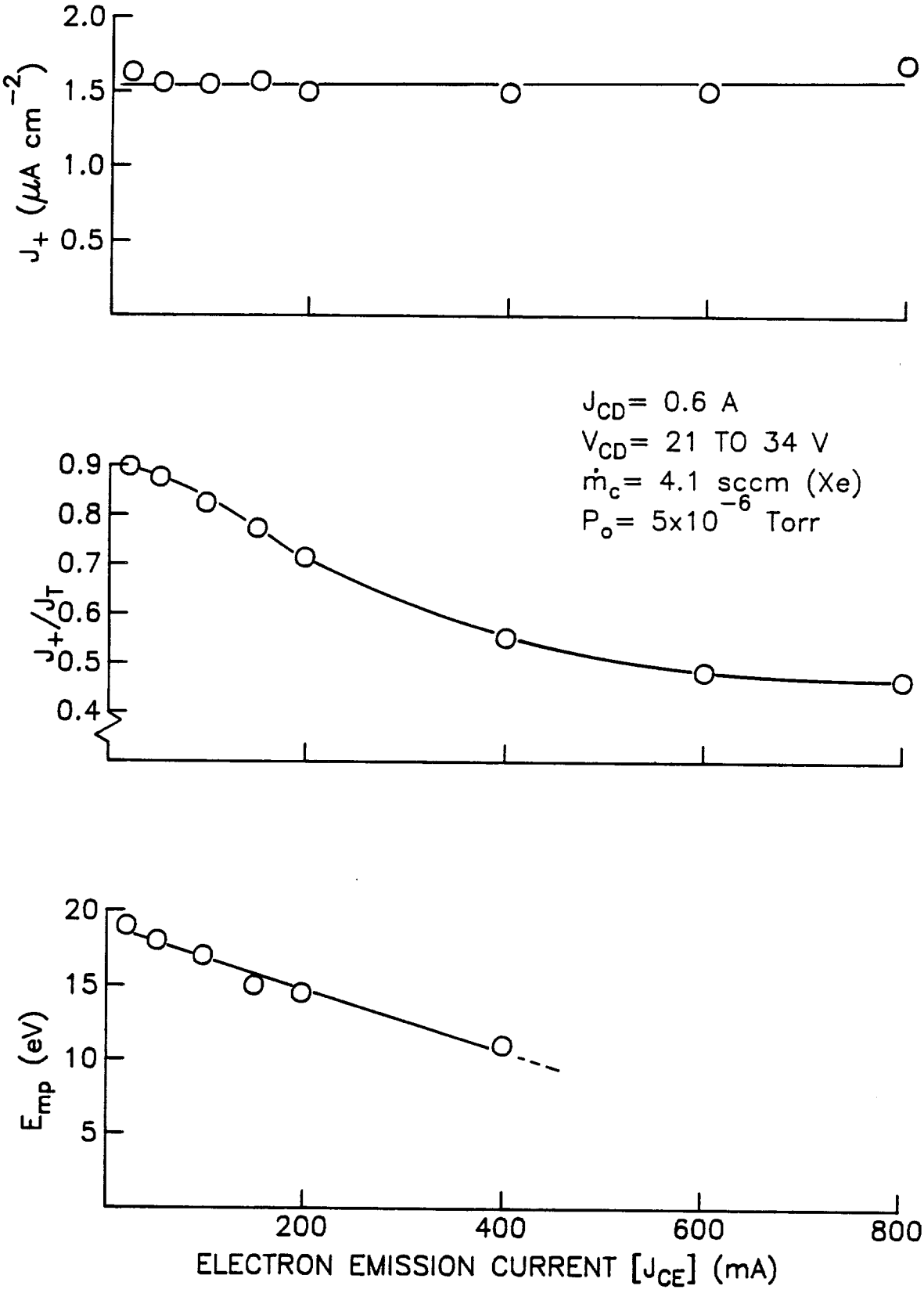

Fig. 15 Effects of Electron Emission Current on Ions Emitted from the Potential Hill

presented in the figure indicate the maximum ion energy and the half width, half maximum energy spread (ΔE) remain at about 50 to 60 eV and 15 to 20 eV, respectively, as emission current is varied over the range of Fig. 15. Examination of the derivatives of the associated RPA data indicate that the ambient and ion emission current density signals become more difficult to distinguish (making determination of E_{mp} difficult) as the electron emission current is increased above 400 mA. The reasons why the ion energy distribution changes as it does with electron emission current and why these changes are different with contactor discharge current are not understood. In addition to effects of contactor discharge and electron emission currents, the contactor flowrate ($\dot{m}_c$) can affect the ion emission current characteristics.

Figure 16 shows the variation in the ion energy distribution parameters identified previously that are induced by changes in contactor flowrate, $\dot{m}_c$. The ion emission current density (J_+) and the ratio of J_+/J_T decrease with increasing flowrate, while E_{mp} remains relatively unchanged. Other data, not shown in Fig. 16, show that the maximum ion energy and the half width, half maximum ion energy spread remain at about 50 to 60 eV and 13 to 20 eV, respectively, over the flowrate range indicated. Just as the behavior reflected in Fig. 14 and 15 was not understood, the reasons why the trends shown in Fig. 16 develop have not been explained at this time.

Simulator Selection Experiments

Several experiments were conducted to compare the performance of five different simulators. The objective of these tests was to determine which simulator design would produce the most desirable ambient plasma (i.e. a low density, uniform, relatively quiescent one).

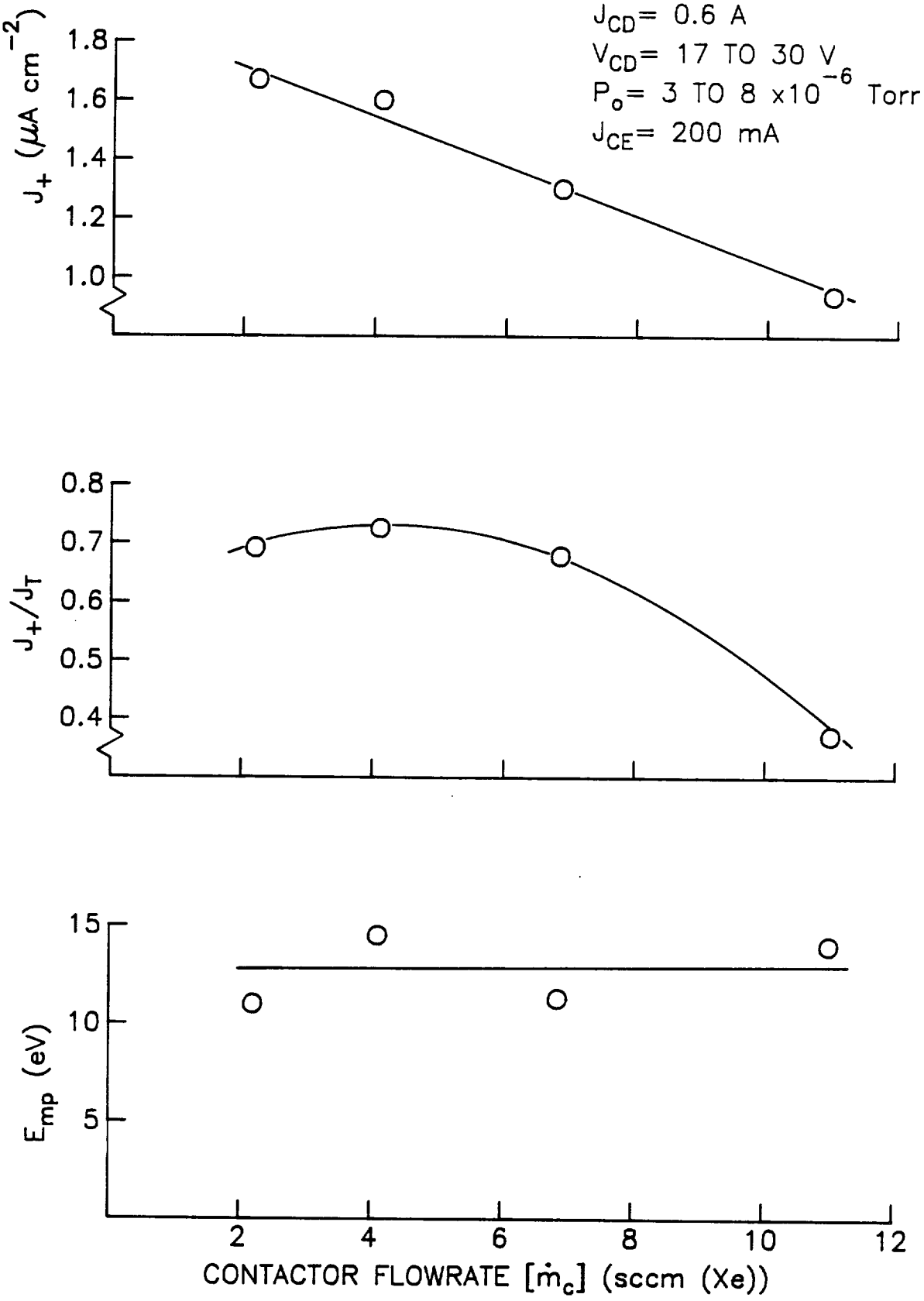

Fig. 16 Effects of Contactor Flowrate on Ions Emitted from the Potential Hill

Electrical schematics of the five simulators investigated are shown in Figs. 7 and 8. The first three designs (Nos. 1, 2, and 3) resemble one another physically, but their electrode designs are different. The No. 1 Simulator is equipped with a loop anode, a loop cathode and a discharge chamber body (9.3 cm dia) that floats. The No. 2 Simulator configuration is similar to that of No. 1, but the discharge chamber body is held at anode potential rather than being allowed to float. The No. 3 Simulator utilizes the discharge chamber body only as an anode, and its cathode is an emissive wire stretched diagonally across the mouth of the discharge chamber (in contrast to the circumferentially oriented loop cathodes used in Nos. 1 and 2). In Simulators 1, 2, and 3, an AC power supply was used to sustain a filament cathode current that would hold its temperature at a value that would yield the desired electron emission current and a discharge current of 0.9 A. The discharge voltage (V_{SD}), which can be set independently in filament cathode plasma sources, was held at 40 V. For Simulators Nos. 4 and 5, which were equipped with a 0.64 cm dia hollow cathode electron source, the discharge voltage was allowed to vary with operating conditions as necessary to sustain a 0.6 A discharge current. These hollow cathode-based simulators used both the discharge chamber body and a 6.5 cm dia loop positioned near the midpoint of the discharge chamber wall as anodes. However, most of the discharge current (over 90%) was collected on the 6.5 cm dia loop anode, and, consequently, holding the chamber body at anode potential or allowing it to float did not affect the discharge chamber plasma conditions significantly.

As mentioned in the Apparatus section of this report, all five simulator configurations employ a ring-cusp magnetic field (see Figs. 5

and 6). This magnetic field is applied to enhance the efficiency of both ion production and the delivery of ions and electrons into the ambient plasma. The magnetic ring-cusp in Simulators 1, 2, and 3 is located near the chamber mouth while it is near the midpoint of the chamber of Simulators 4 and 5. The five simulators were compared in terms of the ambient plasma potential, density and electron temperature they produced throughout the tank when each was supplying ambient plasma for a common contactor collecting electrons (i.e. J_{CE}= -200 mA). In all tests to be described in this section, the simulator electron emission current was collected by a plasma contactor located 2.7 m from the simulator. The plasma contactor was a simple hollow cathode device equipped with a 12 cm dia, flat plate anode. It was operated at 4.1 sccm (Xe) and 0.6 A discharge current. The contactor discharge voltage was about 24 V. In order to reduce arcing problems that could develop at high bias voltage conditions, the vacuum facility was floated relative to the simulator/contactor circuit.

Plasma potential profiles obtained along the centerline are shown in Fig. 17 for Simulators 1, 2, and 3. They extend to positions about 200 cm downstream of the simulators and exhibit widely different characteristics. The poorest simulator in terms of potential difference required to pull 200 mA of electron current from its filament is Simulator No. 2. This could be due to poor plasma production or very effective confinement of electrons within the device. Simulator No. 1 also exhibits poor performance in this sense, but it is more attractive than No. 2 because its intermediate double layer is closer to the simulator -- this allows the ambient plasma to fill a larger portion of the tank thereby assuring it will be more uniform and less likely to

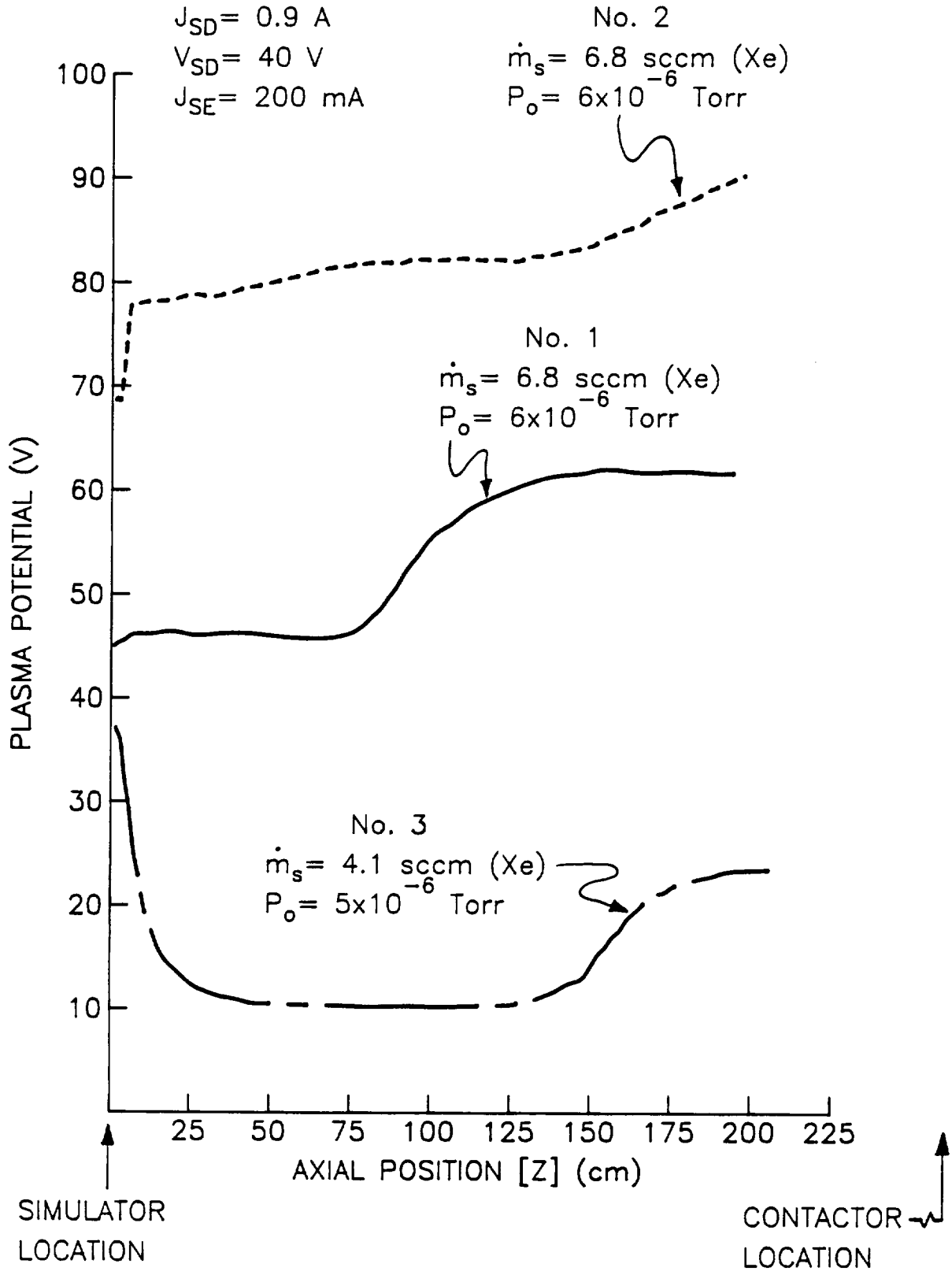

Fig. 17 Plasma Potential Profile Comparison for Simulator Nos. 1, 2, and 3 (Note That Simulator and Contactor Locations have been Switched)

perturb contactor-related phenomena. Simulator No. 3 shows the best performance. In fact the negative potential gradient exhibited at the simulator location suggests it is emitting both ions and electrons. Although the performance of Simulator No. 3 is considered good, the data in Fig. 17 indicate that its intermediate double layer location (~150 cm is farther downstream than that for Simulator No. 1.

Plasma density and electron temperature data comparisons corresponding to the plasma potential profiles in Fig. 17 are shown in Fig. 18. The most important information on these plots is probably the density in the ambient plasma region which is shown at the top of Fig. 18 at axial locations downstream of the intermediate double layer. One of our objectives has been to produce a low density ambient plasma. In this regard, Simulators No. 1 and 2 appear to be best. Thus, a simulator like No. 3 that is desirable in one regard (low plasma potential at the simulator as shown in Fig. 17) appears to be less desirable in another (high ambient plasma density as shown in the upper plot of Fig. 18).

Unlike the plasma density data shown at the top of Fig. 18, the electron temperature data shown at the bottom of Fig. 18 do not appear to display as much structure. The most noticeable trend, however, is a general increase in temperature with increasing downstream position, which is especially noticeably when going from the low to high potential side of the intermediate double layer. This trend is undesirable because a low temperature ambient plasma near the contactor is preferred.

The comparative test of Simulators No. 4 and 5 had to be performed at a higher electron emission current (J_{SE}) than the test for Nos. 1, 2,

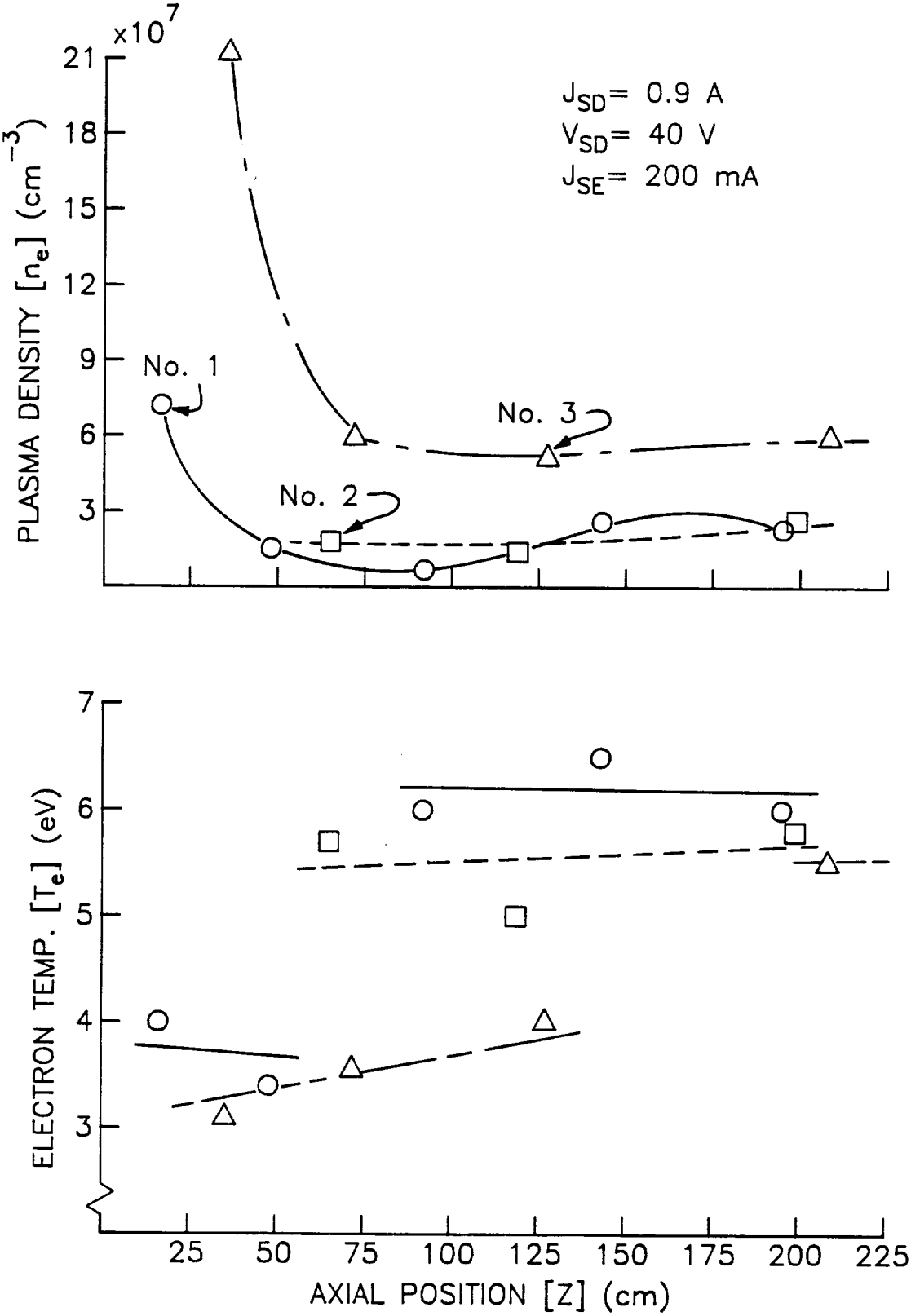

Fig. 18 Plasma Property Comparison for Simulator Nos. 1, 2, and 3

and 3 because of discharge/emission stability problems experienced with Simulator No. 4. This test was performed at J_{SE}= 600 mA and the results are displayed in Fig. 19. The data of Fig. 19 show the effects of moving the hollow cathode from the upstream centerline location (No. 4) to the downstream one (at the chamber mouth -- No. 5) on plasma potential and plasma density profiles. The curves and data points in both plots nearly coincide and this suggests Simulators No. 4 and 5 induce similar ambient plasmas. This is a surprising result because it was expected electrons would have been emitted from the simulator hollow cathode to the contactor more readily when it was near the mouth of the discharge chamber and downstream of the strongest magnetic field regions in the source.

Although the plasma potential and plasma density for the two cases shown in Fig. 19 do not differ significantly, the distribution functions describing the electron populations in the region 10 to 80 cm were quite different. Simulator No. 5 produced a non-Maxwellian plasma there (with an average electron energy between 8 and 12 eV and a spread of about 4 eV), while No. 4 produced a fully Maxwellian plasma (with an electron temperature of 2 to 3 eV). The difference between the two electron distributions in the plasma expansion region could be due to relative ease in which electrons from No. 5 could enter the plasma expansion region. The electron groups downstream of the intermediate double layer (~125 cm) were found to be Maxwellian for both No. 4 and 5 (with a temperature of 5 to 7 eV).

In addition to the experiment discussed above, the noise characteristics associated with the plasma contacting process were studied. An indication of the noise associated with a plasma can be

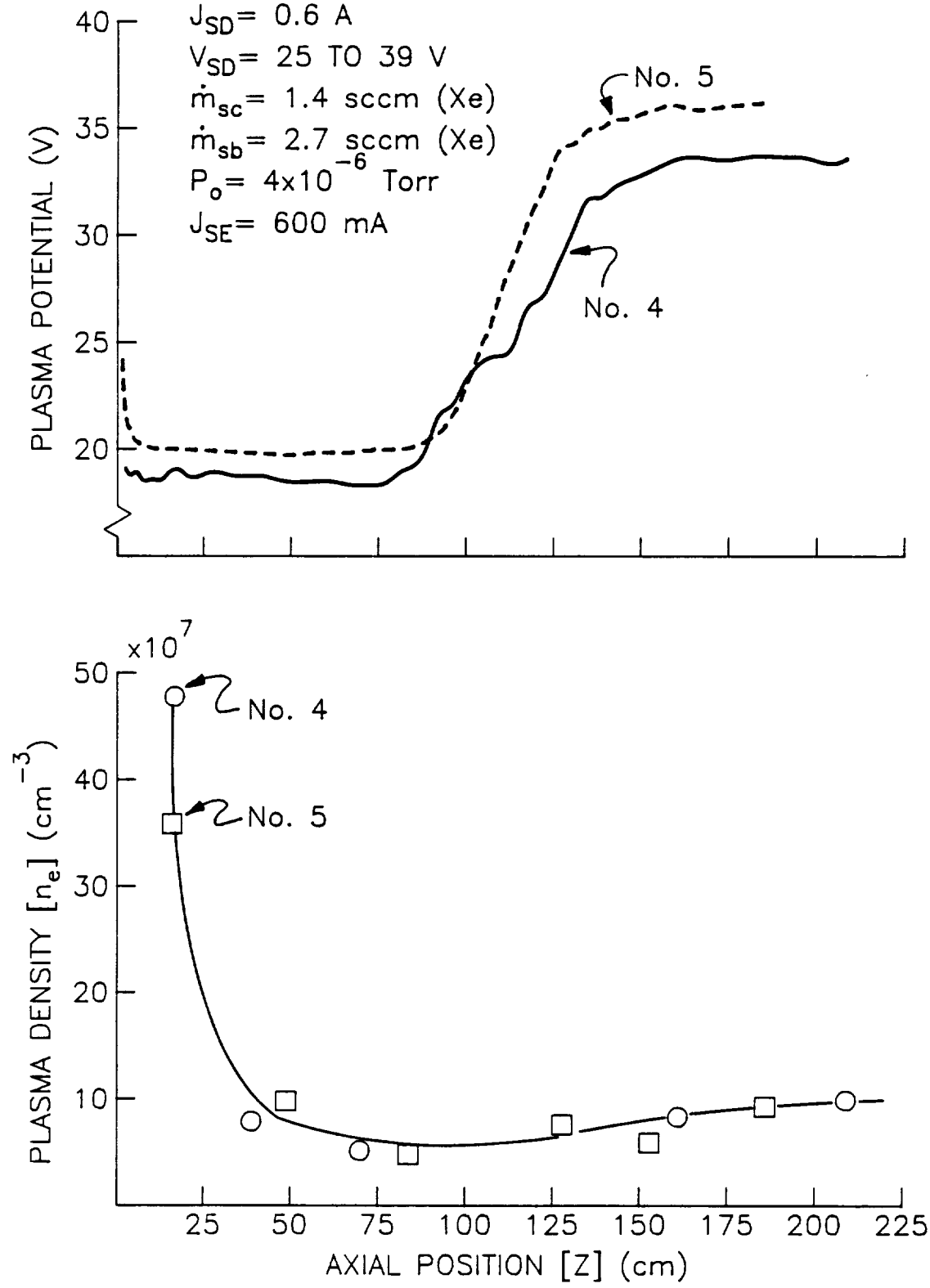

Fig. 19 Comparison of Plasma Property Data for Simulator Nos. 4 and 5

obtained by measuring the electron saturation current to a Langmuir probe with an oscilloscope and noting the ratio of the rms fluctuation-to-average value of this current (i.e. the noise-to-signal ratio). Figure 20 shows the variation in this ratio measured in the ambient plasma region as a function of the electron current being collected from typical ambient plasmas by a hollow cathode-based plasma contactor. The figure compares noise-to-signal ratios obtained using the hot filament-based simulator (Simulator No. 3 -- circle and square data points) to those obtained (triangular data points) using a hollow cathode-based simulator (No. 5). The circle and square data points correspond to hot filament-based simulator operation at flowrates of 2.7 and 4.1 (sccm (Xe)) and are shown to fall below the hollow cathode-based simulator data. The noise-to-signal ratio obtained with the hot filament-based device (e.g. at $|J_{CE}|$= 100 mA, $\dot{m}_s$= 4.1 sccm (Xe)) is seen to be approximately one sixth of the value for the hollow cathode-based device. Since the ratio of turbulent energy stored in a plasma to its total internal energy is proportional to the square of the noise-to-signal ratio, the change from a hollow cathode to a filament cathode simulator induces a great reduction in plasma turbulence level. Specifically, turbulent-to-thermal energy in the ambient plasma produced by the hot filament-based simulator is ~1/36 of that produced by the hollow cathode-based one! The data of Fig. 20 also show that the turbulence level tends to increase with the current being collected by the contactor and with reductions in simulator flowrate ($\dot{m}_s$). In order to assure plasma turbulence levels that are as low as possible and hence plasma property measurement results that are as accurate as possible,

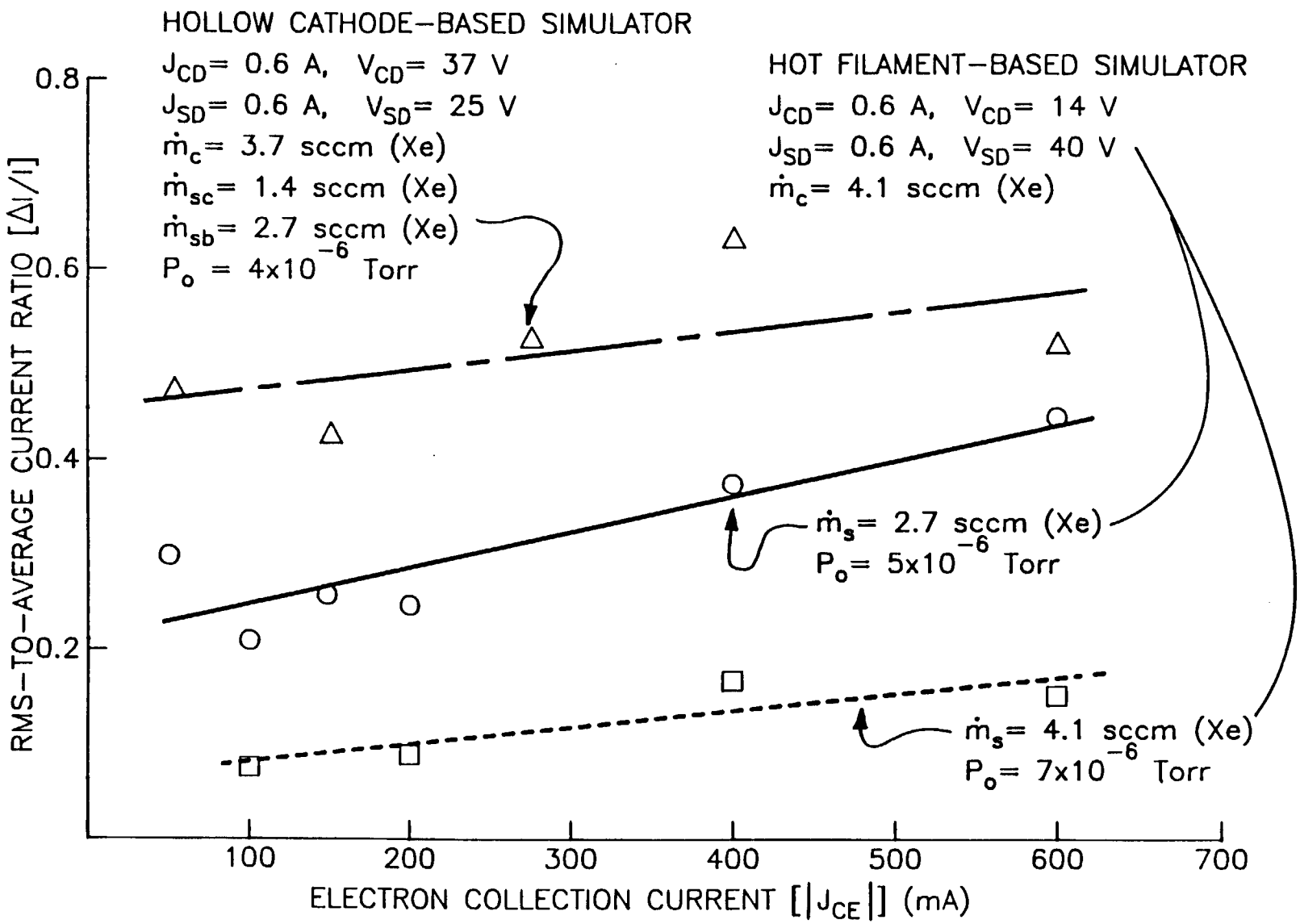

Fig. 20 **Ambient Plasma Turbulence Data: Contactor Collecting Electrons**

the hot filament-based simulator will be used to conduct all future plasma contactor experiments.

CONCLUSIONS

A double layer develops between a plasma contactor collecting electrons and an ambient plasma. The high potential side of the double layer has been observed to host a high energy electron beam which is formed by accelerating ambient electrons through the double layer. Conversely, the low potential side of the double layer is observed to host a high energy ion beam which is formed by accelerating ions from the plasma near the contactor through the double layer. These high energy particles have also been observed by other researchers investigating double layer phenomena. In some electron collection current ranges, simple spherically symmetric models describe the observed current/voltage characteristics of the double layer adequately. More detailed numerical models of the electron collection process can be applied to reproduce most of the phenomena observed in the experiments. Although some experiments carried out at NASA LeRC have indicated that simple one dimensional models fail to describe the phenomena observed at high electron collection in their facility, recent experiments conducted under this grant suggest that the simple models are still adequate up to ~3 A. Some of the inconsistencies between the two experiments might be explained by the lower neutral densities at NASA LeRC (50% lower) and the possibility that the intermediate double layer moves to the point where it interacts with the contactor double layer.

High energy ion emission is observed coming from a hollow cathode operating in the electron emission mode. Originally, it was considered

unlikely that a contactor emitting electrons could also emit ions. Subsequently, a process was postulated that involves a high ionization rate near a hollow cathode emitting electrons. It is suggested that this high ionization rate causes ion space charge build-up to the point where a region of high potential develops. Ions produced near the top of the potential hill can flow from it into the expanding plasma region and gain substantial energy. It is believed that energy conservation criteria and the ion/electron production and loss balance condition describe and limit this process. Although, ion emission characteristics from the potential hill have been measured, they have not been fully explained in terms of contactor operating conditions.

A plasma source has been selected to produce a low noise, relatively uniform ambient plasma. The device is a simple ring cusp ion source which is equipped with a hot filament cathode that is stretched diagonally across its mouth. The device produces an ambient plasma that exhibits plasma noise that is about one fortieth of that produced by a similar hollow cathode-based plasma source. In spite of this lower noise capability, preliminary experiments have indicated that there are no significant differences between plasma property and performance data measured using the hollow cathode and filament-based plasma sources to produce the ambient plasma. Additional experiments are necessary, however, to judge more accurately the effects of ambient plasma noise levels on the performance of hollow cathode-based plasma contactors.

REFERENCES

1. Williams, J., "Electrodynamic Tether Plasma Contactor Research," appears in "Space Plasma Contactor Research - 1987," P. Wilbur, ed., NASA CR-182148, Jan. 1988, pp. 1-78.

2. Patterson and Aadland, "Ground-based Plasma Contactor Characterization," appears in "Space Tethers for Science in the Space Station Era," L. Guerriero and I. Bekey, eds., Societa Italiana Di Fisica, V. 14, Venice, Italy, Oct. 4-8, 1987, pp. 261-268.

3. Martinez-Sanchez, M., and D. Hastings, "A Systems Study of a 100kW Tether, J. of Astro. Sciences, V. 35, 1987, pp. 75-96.

4. Olsen, R., "Experiments in Charge Control at Geosynchronous Orbit -- ATS-5 and ATS-6," J. Spacecraft and Rockets, 22, 1985, pp. 254-259.

5. Vannaroni, G., U. Guidoni, I. Durrani, and F. De Venuto, "Data Analysis of Hollow Cathode Experiment to Support Electrodynamic Tether Applications," Istituto D. Fisica Dello Spazio Interplanetario, Frascati, Italy, Sept. 1989.

6. Hershkowitz, N., "Review of Recent Laboratory Double Layer Experiments," Space Science Reviews, V. 41, 1985, pp. 351-391.

7. Guyot, M., and Ch. Hollenstein, "Experiments of Potential Gradients in a Current-Carrying Plasma. I. Potential Structures," Phys. Fluids, V. 26, No. 6, 1983, pp. 1596-1605.

8. Baker, K., et. al., "Studies of Strong Laboratory Double Layers with Computer Simulation," J. Plasma Physics, V. 26, Part 1, 1981, pp. 1-27.

9. Hershkowitz, N., G. Payne, C. Chan, J. DeKock, "Weak Double Layers," Plasma Physics, V. 23, No. 10, 1981, pp. 903-925.

10. Borovsky, J., and G. Joyce, "The Simulation of Plasma Double Layer Structures in Two Dimensions," J. of Plasma Physics, V. 29, Part 1, 1983, pp. 45-84.

11. Leung, P., A. Wong, and B. Quon, "Formation of Double Layers," Phys. Fluids, V. 23, No. 5, 1980, P. 992-1004.

12. Hatakeyama, R., Y. Suzuki, and N. Sato, "Formation of Electrostatic Potential Barrier Between Different Plasmas," Phys. Rev. Lett., V. 50, No. 16, April 18, 1983, pp. 1203-1206.

13. Williams, J. and P. Wilbur, "Ground-Based Tests of Hollow Cathode Plasma Contactors," Proc. of Third International Conference on Tethers in Space: Toward Flight, San Francisco, AIAA Paper No. 89-1558-CP, May 17-19, 1989, pp. 77-87.

14. Davis, V., I. Katz, M. Mandell, and D. Parks, "A Model of Electron Collecting Plasma Contactors," Submitted to J. of Spacecraft and Rockets, preview paper dated Oct. 3, 1989.

15. Wei, R. and P. Wilbur, "Space-Charge-Limited Current Flow in a Spherical Double Sheath," J. of Appl. Phys., V. 60, No. 7, Oct. 1, 1986, pp. 2280-2289.

16. Williams, J., P. Wilbur, J. Monheiser, "An Experimental Validation of a Phenomenological Model of the Plasma Contacting Process," appears in "Space Tethers for Science in the Space Station Era," L. Guerriero and I. Bekey, eds., Societa Italiana Di Fisica, V. 14, Venice, Italy, Oct. 4-8, 1987, pp. 245-253.

17. Wilbur, P., and J. Williams, "An Experimental Investigation of the Plasma Contacting Process," AIAA paper No. 87-0571, Reno, Nevada, Jan. 12-15, 1987.

18. Chan, C., N. Hershkowitz, and K. Lonngren, "Electron Temperature Differences and Double Layers," Phys. Fluids, V. 26, No. 6, 1983, pp. 1587-1595.

19. Coakley, P., and N. Hershkowitz, "Laboratory Double Layers," Phys. Fluids, V. 22, No. 6, 1979, pp. 1171-1181.

20. Boyd, R., "The Collection of Positive Ions by a Probe in an Electrical Discharge," Proc. Roy. Soc., V. 201A, 1950, pp. 329-347.

21. Crawford F. "Modulated Langmuir Probe Characteristics," J. Appl. Phys., V. 34, No. 7, 1963, pp. 1897-1902.

22. Hershkowitz, N., "How Langmuir Probes Work," appears in Plasma Diagnostics: Discharge Parameters and Chemistry," O. Auciello and D. Flamm, eds., V. 1, Academic Press Inc., New York, pp. 113-183, 1989.

23. Laupa, T., "Electrodynamic Tether Plasma Contactor Research," appears in "Advanced Electric Propulsion and Space Plasma Contactor Research," P.J. Wilbur, ed., NASA CR-175119, Jan. 1986, pp. 39-66.

24. Aston, G., and P. Wilbur, "Ion Extraction from a Plasma," J. Appl. Phys., V. 52, No. 4, 1981, pp. 2614-2626. See also J. Smith, N. Hershkowitz, and P. Coakley, "Inflection-Point Method of Interpreting Emissive Probe Characteristics," Rev. Sci. Instrum., V. 50, No. 2, 1979, pp. 210-218.

25. Langmuir, I., "The Collected Works of Irving Langmuir," C. Suits, ed., V. 3, 4, & 5, Pergamon Press, 1961. See also Beattie, J., "Numerical Procedure for Analyzing Langmuir Probe Data," AIAA Journal, V. 13, No. 7, 1975, pp. 950-952.

26. Brophy, J. and P. Wilbur, "An Experimental Investigation of Cusped Magnetic Field Discharge Chambers," International Electric Propulsion Conference, IEPC 84-70, Tokyo, Japan, 1984.

27. Siegfried, D. "A Phenomenological Model for Orificed Hollow Cathodes", appears in "Advanced Electric Propulsion Research," P.J. Wilbur, ed., NASA CR - 168026, 1982.

28. Allen, J.E., R.L.F. Boyd, and P. Reynolds, "The Collection of Positive Ions by a Probe Immersed in a Plasma," Proc. Phys. Soc., Vol. 70B, 1957, pp. 297-304.

29. Chen, F.F. "Numerical Computations for Ion Probe Characteristics in a Collisionless Plasma," Plasma Physics (Journal of Nuclear Energy Part C), Vol. 7, 1965, pp. 47-67.

APPENDIX A

Langmuir Probe Diagnostics at Low Plasma Densities

Most of the initial work on determining plasma properties from electrostatic probes was performed and explained by Irving Langmuir [25]. He concentrated on plasmas with densities on the order of 10^9 cm^{-3} and electron temperatures on the order of 1 eV. In moderate to dense plasmas like these, the ion current flowing to the probe when it is negative with respect to plasma potential is very small compared to the electron saturation current -- the electron current flowing to the probe when it is biased at plasma potential. The ratio of this ion current-to-electron saturation current was typically less than 1/400 for the mercury plasmas Langmuir studied, and he showed that, in general, this ratio was proportional to the square-root of the electron/ion mass ratio. In addition to this result, Langmuir observed that the ion current flowing to the probe typically saturated (i.e. remained constant) at probe potentials less than ~20 V negative of plasma potential. This result is also observed in most ion thruster discharge chambers and, in fact, it is used to determine the plasma properties in very dense plasmas where biasing the probe to plasma potential would cause the probe to collect too much current and burn out [27]. The magnitude of the ion current that will be collected at negative probe potentials is, however, greatly influenced by the ratio of probe radius-to-plasma Debye length, ξ_p. For the large values of this parameter observed in Langmuir's experiments, the ion collecting sheath which

develops around the probe is very thin and its area is approximately equal to the probe surface area. Because ions flow at the Bohm velocity when they reach the sheath edge of a negatively biased surface, the ion current will saturate if the sheath is thin and ξ_p is large. However, if the probe radius/Debye length ratio is small, then the sheath surrounding the probe will grow and the ion current will increase with decreasing probe potential. This regime of small values of ξ_p (i.e. $\xi_p < 1$) is typically referred to as the thick sheath regime.

A typical Langmuir probe current/voltage trace is shown in Fig. A1. The probe used to collect these data had a radius of 0.159 cm, and it was in a nearly Maxwellian plasma having a density and electron temperature of approximately 5.2×10^6 cm^{-3} and 5.1 eV, respectively. Therefore, the Debye length was ~0.74 cm and the ratio of probe radius-to-Debye length was 0.214. Figure A1 is a typical example of a plot of electron current versus probe voltage measured with respect to plasma potential in this plasma. Consequently, net negative currents occur when the rate of ion arrival to the probe exceeds the rate of electron arrival. At potentials less than -20 to -25 V, one would expect nearly all electrons would be repelled and most of the current to the probe would be due to ions. The figure shows, however, that the probe current varies linearly with probe potential at probe potentials less than ~-25 V. This suggests the trace was collected in the thick sheath regime. A more certain test involves computing the ratio of the magnitudes of the ion current (at some reasonable negative potential) and the electron saturation current. Using the value of ion current at -65 V this ratio can be computed to be 1/4.8 -- a value about 100 times larger than the thin sheath ratio!

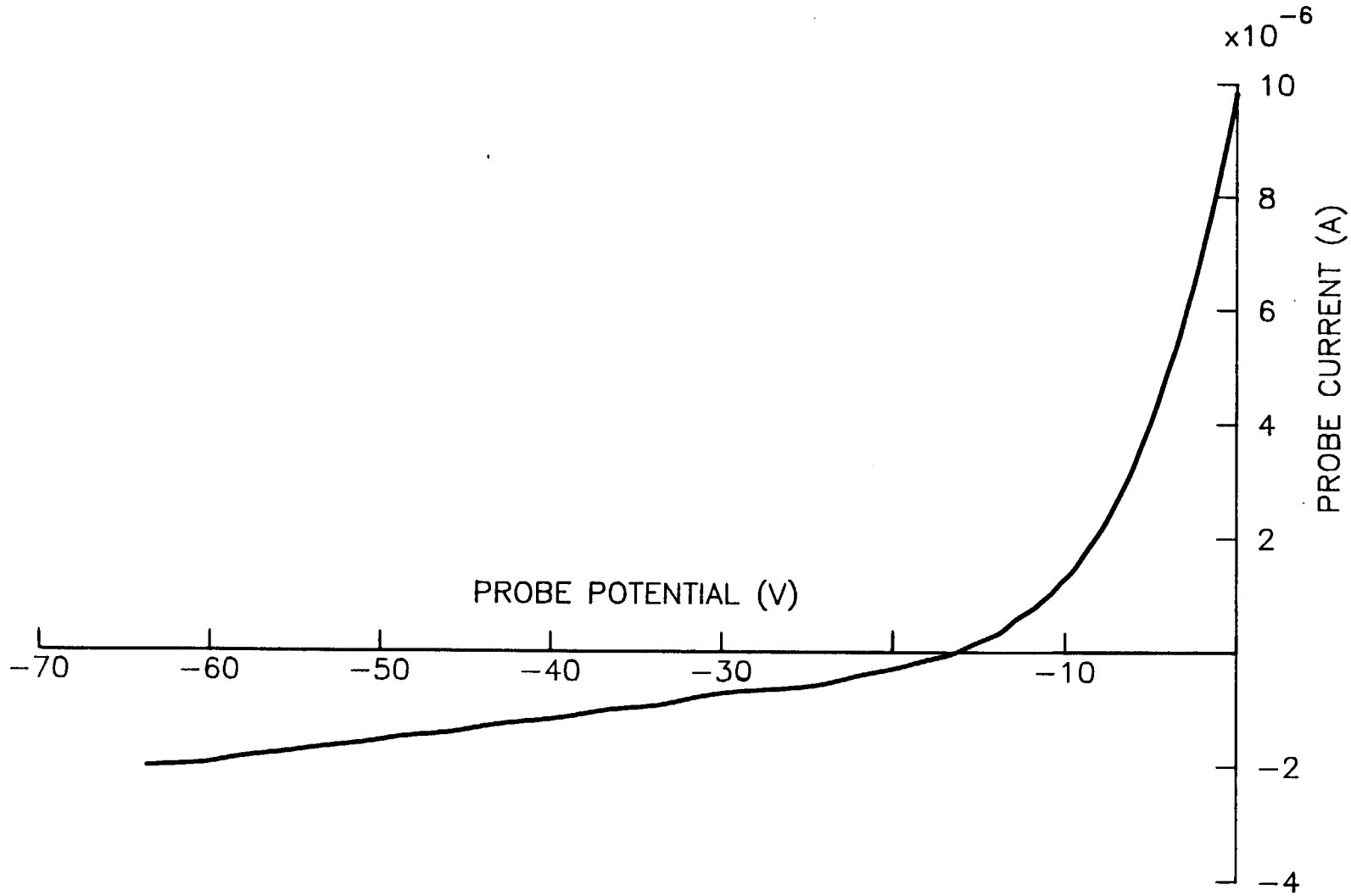

Fig. A1 Typical Thick Sheath Langmuir Probe Trace

Although the ion current seems to be incredibly large, its magnitude and slope can be explained using a relatively simple model of Allen, et.al. [28] and F.F. Chen [29]. The nomenclature and problem formulation are summarized below. It is noted that the nomenclature and variables are similar to those used by Chen for the sake of consistency. Standard International (SI) units will be used throughout the development given here.

Nomenclature:

Physical Constants and Parameters

a - Probe radius (spherical geometry) (m)

r - Radial position measured with respect to the center of the probe (m)

λ_D - Plasma Debye length = $\left[\frac{\epsilon_o kT_1}{e_1^2 n_{1o}} \right]^{1/2}$ (m)

T_1 - Temperature of repelled particles (electron temperature) (K)

n_{1o} - Density of repelled particles measured far from probe (m^{-3})

ϵ_o - Permittivity of free space (F/m)

k - Boltzmann constant (J/K)

e_1 - Charge of repelled particles (electron charge) (C)

e_2 - Charge of attracted particles (ion charge) (C)

m_2 - Mass of attracted particle (kg)

I_2 - Ion current flowing to probe (A)

V - Probe potential measured with respect to plasma potential (V)

ξ - Non-dimensional length = r/λ_D

η - Non-dimensional potential = $\frac{e_1 V}{k T_1}$

$$J \text{ - Non-dimensional ion current} = \frac{I_2}{\frac{4\pi\epsilon_o}{e_2}\,(2/m_2)^{1/2}\,(kT_1)^{3/2}}$$

If one assumes that the ions are cold (i.e. have negligible velocity) far away from the probe, and that they do not experience any collisions as they approach the probe, the following equations can be used to describe the potential variation around the probe.

Poisson's Equation --

$$\frac{1}{r^2}\frac{d}{dr}\left(r^2\frac{dV}{dr}\right) = \frac{-n_1e_1 - n_2e_2}{\epsilon_o} \qquad (1)$$

Electron Density-

$$n_1 = n_{1o}\exp(-\eta) \qquad (2)$$

Ion Density-

$$n_2 = \frac{I_2}{4\pi r^2 e_2\left[\frac{-2\,e_2\,V}{m_2}\right]^{1/2}} \qquad (3)$$

Substitution of Eqs. (2) and (3) into Eq. (1) and application of the non-dimensional definitions of length, potential and ion current yields

$$\frac{d^2\eta}{d\xi^2} + \frac{2}{\xi}\frac{d\eta}{d\xi} + \exp(-\eta) = \frac{J}{\eta^{1/2}\,\xi^2} \quad . \qquad (4)$$

F.F. Chen [29] provides graphical solutions to Eq. (4) over a wide range of non-dimensional current (J), but does not include solutions for values of J between 0.1 and 5 -- the range into which plasma contactor plasma data have typically fallen. In order to extend Chen's work a program was written to solve Eq. 4. Typical results obtained from this program showing the variation of ξ with η for values of J between 0.1 and 5 are given in Fig. A2. The data of Fig. A2 are used by first drawing a vertical line at the value of ξ corresponding to the probe radius (e.g. at $\xi_p = 0.214$ for the data shown in Fig. A1) and then

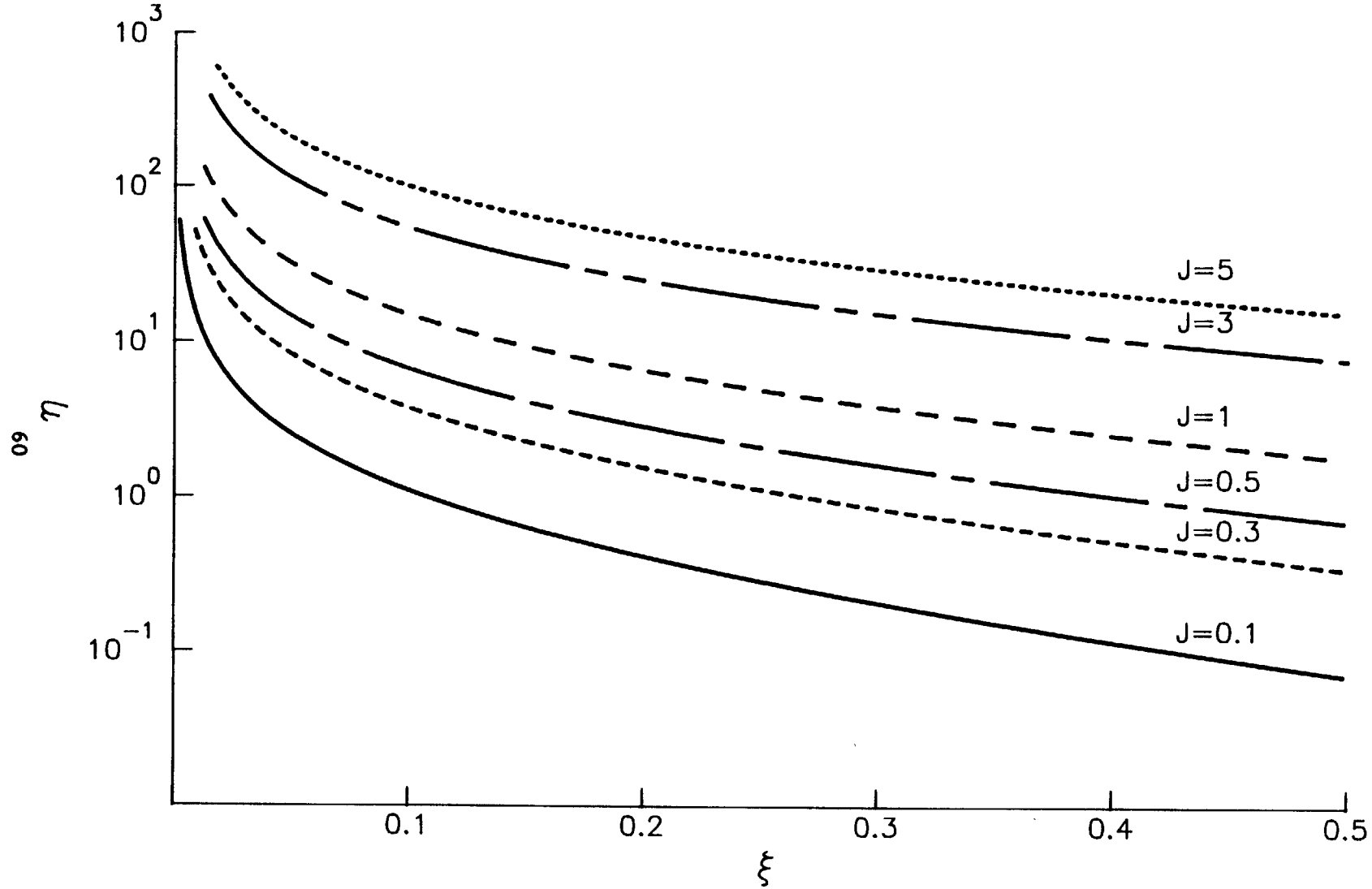

Fig. A2 Non-Dimensional Probe Potential vs. Non-Dimensional Probe Size

picking off values of non-dimensional probe potential (η) as a function of non-dimensional probe current (J).

If this is done for $\xi_p = 0.214$ the non-dimensional ion current versus non-dimensional probe potential, data represented by the circular symbols in Fig. A3 are obtained. The square symbols represent experimental voltage/current data points that have been taken directly from Fig. A1 and expressed in non-dimensional form. The slopes of the two curves are seen to be the same. This suggests that the essential physics inherent in the data of Fig. A1 is represented in Eqs. (1) through (4). However, the magnitudes of the ion currents determined from the theory differ from those measured experimentally. There are several possible reasons why this difference might have developed. They include 1) errors in measuring plasma density and/or electron temperature and plasma potential, 2) the effect of non-zero initial ion velocities (accounting for this effect requires the consideration of ion orbital motion near the probe and this complicates the analysis) and 3) a non-Maxwellian electron distribution superimposed on the Maxwellian electron distribution (e.g. the presence of high energy, mono-energetic electrons).

Although the two curves shown in Fig. A3 do not agree completely, some observations can be made. The most surprising one is that the theory predicts ion currents which are even greater than the ones measured experimentally! The theory also predicts that the ion current should vary almost linearly with potential and this is in agreement with experimental results. This result was unexpected because of the highly non-linear form of the governing equation (Eq. (4)).

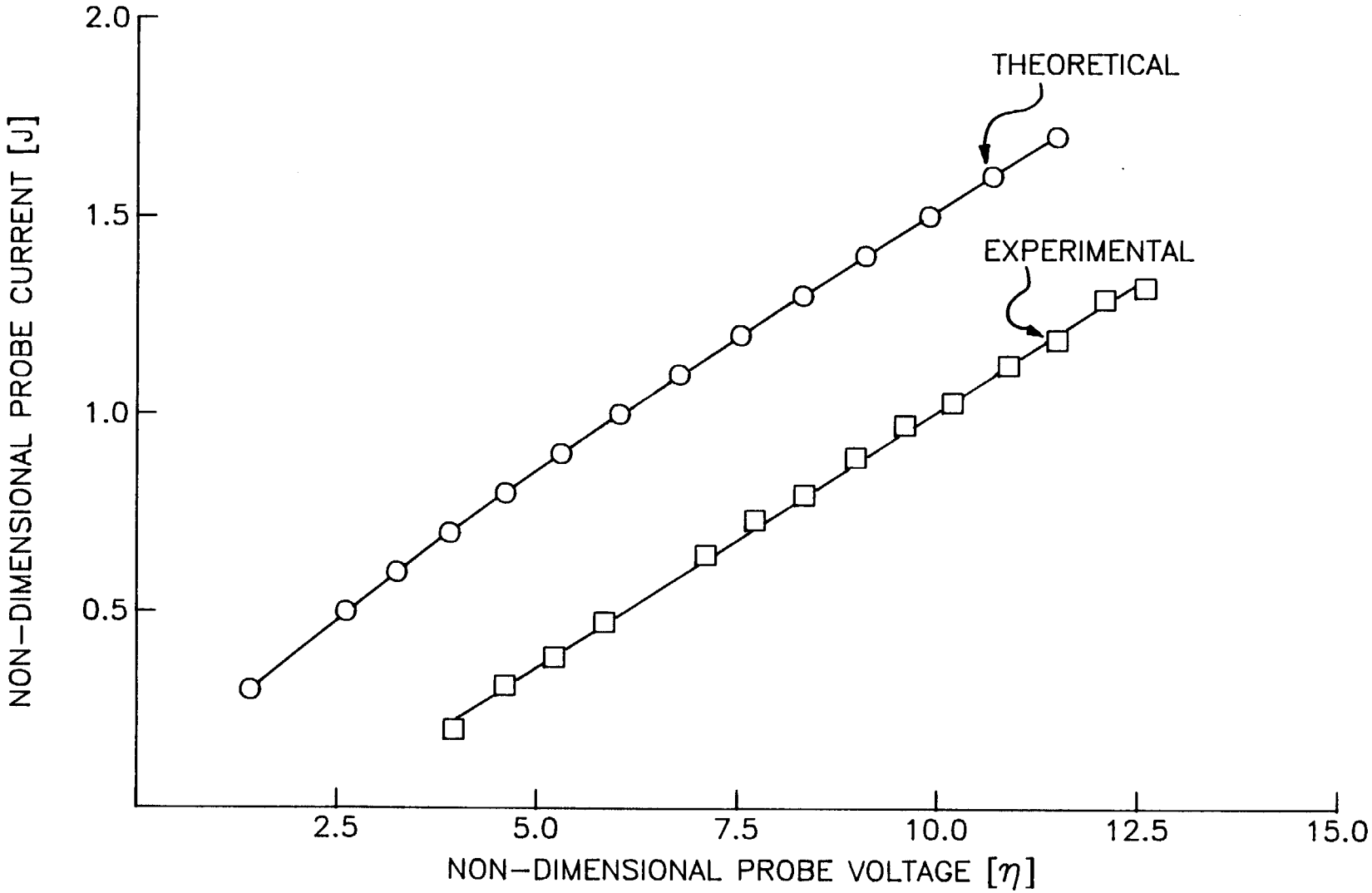

Fig. A3 Non-Dimensional Langmuir Probe Data in the Ion Collection Regime

DISTRIBUTION LIST

	Copies
National Aeronautics and Space Administration Washington, DC 20546 Attn:	
Mr. Edward J. Brazill, Code MD	1
Mr. Thomas D. Stuart, Code MK	1
Dr. Stanley Shawhan, Code ES	1
Dr. L.R. Owen Storey, Code ES	1
Mr. George Levine, Code MTF	1
Mr. Ivan Bekey, Code Z	1
Mr. John L. Anderson, Code RS	1
National Aeronautics and Space Administration Lewis Research Center 21000 Brookpark Road Cleveland, OH 44135 Attn:	
Technology Utilization Office, MS 7-3	1
Report Control Office, MS 60-1	1
Library, MS 60-3	2
Dr. M. Goldstein, Chief Scientist, MS 5-9	1
Mr. Dave Byers, MS 500-219	1
Mr. Vincent Rawlin, MS 500-220	1
Dr. Carolyn Purvis, MS 302-1	1
Mr. Joseph C. Kolecki, MS 501-6	1
Mr. Michael Patterson, MS 500-220	1
Dr. Dale Ferguson, MS 302-1	1
Mr. Norman T. Grier, MS 302-1	1
Mr. Joel T. Galofaro, MS 302-1	10
National Aeronautics and Space Administration Lyndon B. Johnson Space Center Houston, TX 77058 Attn:	
Dr. James E. McCoy, Mail Code SN3	1
National Aeronautics and Space Administration Marshall Space Flight Center Huntsville, AL 35812 Attn:	
Mr. J. H. Laue, Mail Code FA31	1
Mr. Chris Rupp, Mail Code PS04	1
Mr. James K. Harrison, Mail Code PS04	1
NASA Scientific and Technical Information Facility P.O. Box 8757 Baltimore, MD 21240 Attn:	
Accessioning Dept.	1

	Copies
Dept. of the Navy Office of Naval Research University of New Mexico Bandolier Hall West Albuquerque, NM 87131 Attn:	
G. Max Irving	1
Procurement Executive, Ministry of Defense Royal Aircraft Establishment Farnborough, Hants GU14 6TD ENGLAND Attn:	
Dr. D. G. Fearn	1
United Kingdom Atomic Energy Authority Culham Laboratory Abingdon, Oxfordshire OX143DB ENGLAND Attn:	
Dr. A. R. Martin (Rm F4/135)	1
Defense Nuclear Agency DNA/RAEV Washington, D.C. 20305-1000 Attn:	
Captain Daniel Allred	1
SRT Technologies 1500 Wilson Blvd, Suite 800 Arlington, VA 22209-2415 Attn:	
Ms. Kaye Anderson	1
Air Force Astronautics Lab Edwards AFB, CA 93523 Attn:	
LKDH/Lt. Robert D. Meya, MS 24	1
LKDH/Lt. Phil Roberts, MS 24	1
Jet Propulsion Laboratory 4800 Oak Grove Laboratory Pasadena, CA 91109 Attn:	
Technical Library	1
Dr. John R. Brophy	1
Dr. Paul Penzo, Code 1156-217	1
Dr. Stephen Gabriel	1

	Copies
TRW Inc. TRW Systems One Space Park Redondo Beach, CA 90278 Attn:	
Mr. Neal Holkower	1
Dr. Rob Stillwell	1
National Aeronautics and Space Administration Ames Research Center Moffett Field, CA 94035 Attn:	
Technical Library	1
National Aeronautics and Space Administration Langley Research Center Langley Field Station Hampton, VA 23365 Attn:	
Technical Library	1
Mr. George Wood, Mail Code 234	1
Hughes Research Laboratories 3011 Malibu Canyon Road Malibu, CA 90265 Attn:	
Dr. Jay Hyman, MS RL 57	1
Dr. J. R. Beattie, MS RL 57	1
Dr. J. N. Matossian, MS RL 57	1
Rocket Research Co. P.O. Box 97009 Redmond, WA 98073-9709 Attn:	
Mr. William W. Smith	1
Mr. Paul Lichon	1
Mr. Lee Parker 252 Lexington Road Concord, MA 01741	1
Department of Aeronautics and Astronautics Massachusetts Institute of Technology Cambridge, MA 02139 Attn:	
Dr. Daniel E. Hastings, Rm 37-441	1
Institute for Space and Aeronautical Science 4-6-1 Komaba, Meguro-ku, Tokyo, 153, JAPAN Attn:	
Prof. K. Kuriki	1
Prof. T. Obayashi	1

	Copies
Tokai University Kitakauame, Hiratsuka, Kanagawa, JAPAN Attn:	
Prof. K. Hirao	1
Physics Department Naval Postgraduate School Monterey, CA 93943-5000 Attn:	
Dr. Chris Olson, Mail Code 61-0S	1
Martin Marietta Aerospace P. O. Box 179 Denver, CO 80201	1
Attn:	
Dr. Kevin Rudolph, MS M0482	1
S-Cubed P. O. Box 1620 LaJolla, CA 92038	1
Attn:	
Dr. Ira Katz	1
Dr. Victoria Davis	1
Electric Propulsion Laboratory, Inc. 43423 N. Division St., Suite 205 Lancaster, CA 93535 Attn:	
Dr. Graeme Aston	1
Mr. Joe Carroll Energy Science Laboratories, Inc. P.O. Box 85608 San Diego, CA 92138-5608	1
Instituto du Fisica dello Spazio Interplanetario Consiglio Nazionale dello Richerche Via G. Galilei 00044 Frascati, ITALY Attn:	
Dr. Marino Dobrowolny	1
Dr. Carlo Bonifazi	1
Dr. Luciano Iess	1
Mr. Giuliano Vannaroni	1
Science Applications International Corp. 13400 B Northrop Way #36 Bellevue, WA 98005 Attn:	
Dr. Hugh Anderson	1

	Copies
Starlab/SEL Stanford University Stanford, CA 94305 Attn:	
Dr. Peter Banks	1
Dr. Roger Williamson	1
Science Applications International Corp. Plasma Physics Division 1710 Goodridge Drive McLean, VA 22102 Attn:	
Mr. Edward P. Szuszczewicz	1
University of Alabama (Huntsville) Electrical and Computer Engineering Dept. Engineering Building Huntsville, AL 35899 Attn:	
Dr. Michael Greene	1
Physics Department Utah State University Logan, Utah 84322 Attn:	
Dr. W.J. Raitt	1